

BELLCOMM, INC.

955 L'ENFANT PLAZA NORTH, S.W.

WASHINGTON, D. C. 20024

COVER SHEET FOR TECHNICAL MEMORANDUM**TITLE-** Simulation of Surveyor Strain Gage Data**TM-**68-1014-8**DATE-** October 9, 1968**FILING CASE NO(S)-** 340**AUTHOR(S)-** E. N. Shipley**FILING SUBJECT(S)-****(ASSIGNED BY AUTHOR(S)-**

LM

Landing Dynamics

Landing Simulations

Lunar Surface Properties

Soil Mechanics

Surveyor

ABSTRACT

This memorandum deals with the interpretation of the strain gage data received from Surveyor spacecraft during their landing on the lunar surface. Digital computer simulations of the Surveyor landing have been carried out using a soil model which is consistent with the data obtained from Surveyors I and III. The use of a soil model is of value because it provides a means of extending the information obtained about the lunar surface to the landings of other spacecraft having different dimensions, weights and touch-down conditions.

Analysis of the strain gage data provides results which agree with previous findings, but because of the lack of knowledge of the horizontal forces acting on the footpad, it is not possible to extend the analysis to determine the parameters describing the detailed properties of the soil model.

In addition, the effect of the filter in the strain gage telemetry channel is studied. It is found that it does not alter the observed traces or the interpretation of the data to a significant extent.

(NASA-CR-73512) SIMULATION OF SURVEYOR
STRAIN GAGE DATA (Bellcomm, Inc.) 55 p

N79-73392

Unclas
12681

00/91

FF No. 602

73512

(NASA CR OR TMX OR AD NUMBER)

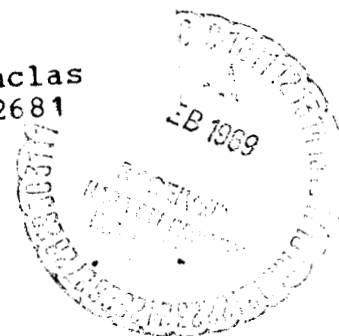
(CODE)

30

(CATEGORY)

SEE REVERSE SIDE FOR DISTRIBUTION LIST

BA-145A (3-67)



SUBJECT: Simulation of Surveyor
Strain Gage Data
Case 340

DATE: October 9, 1968

FROM: E. N. Shipley

TM-68-1014-8

TECHNICAL MEMORANDUM

1.0 INTRODUCTION

1.1 Background

This memorandum concludes a series of studies which have dealt with the simulation of a Surveyor spacecraft landing on the lunar surface. The underlying purpose of these studies has been to interpret the data obtained from the Surveyor Program in terms of the properties of the lunar surface material. The landing performance of the Apollo Lunar Module (LM) has also been estimated, particularly in materials whose properties were chosen to agree with the results of Surveyor I.

The previously reported work^(1,2) has dealt primarily with the penetration of the Surveyor footpads into the lunar surface during the landing process. The depth of penetration of the footpads can be measured by means of television pictures obtained from the spacecraft subsequent to its landing.

This memorandum deals with the interpretation of the data which are obtained from strain gages attached to the Surveyor shock absorbers. During the landing of the spacecraft, the force level in each of the three shock absorbers on the spacecraft is telemetered to the earth-based receiving station. We will refer to the shock absorber force as a function of time as a "strain gage trace" or as the "strain gage data" because of its origin in the strain gage on the shock absorber.

Beginning with the third spacecraft there was a change in the shock absorber design which produces a significant effect on the strain gage data. The shock absorber for Surveyor I and that for Surveyor II, which was unsuccessful, will be referred to as the "old" shock absorber, and that for Surveyor III and all subsequent spacecraft as the "new" shock absorber. Results from both of these shock absorbers are included in the present study.

There are two principal technical sections to this memorandum. In Section 2, the strain gage traces generated by a computer simulation of a Surveyor spacecraft landing on a model

lunar soil are described and compared to the data obtained from Surveyor I. In Section 3, the effect of the telemetry channel, and specifically the effective passive filter between the strain gage itself and the recorded data, is considered. Because the effect of the filter on the telemetry channel is small, it has been possible to delay this discussion until after the strain gage traces themselves have been discussed. The second part of the Introduction is concerned with a brief discussion of the soil model and the simulation procedures.

An important feature of this work is the use of a realistic soil model to describe the forces between the footpad and the lunar surface. This allows a description of the soil in terms of quantities such as internal friction, cohesion and density. Furthermore, the soil model used here includes dynamic effects within the soil.

In our case, the use of a soil model is important because it provides a direct way of predicting force levels for footpads with dimensions different from those of Surveyor. In general, the bearing capacity of a soil depends on the size of the footpad, and it is only through the properties of the soil model that one is able to extrapolate the properties deduced from Surveyor data to an estimate of the performance of a LM landing on the moon. The value of the extrapolation naturally depends on the adequacy of the soil model in describing the behavior of the lunar soil. The soil model which has been used in these studies appears to be consistent with all observations obtained by Surveyor I and Surveyor III. However, the soil model should at this stage only be considered to be a working hypothesis.

Considerable work has previously been done both by Sperling and Garba at JPL³ and by Jones at Hughes Aircraft Company⁴ on the interpretation of strain gage traces from Surveyor. They have also developed computer simulation programs for the Surveyor landing, and have used a much more complete model of the spacecraft than has been possible in the studies reported here. Perhaps the most significant advantage in their studies is the freedom to consider landings on sloping surfaces. The simulations reported here require the spacecraft roll axis to remain fixed parallel to the gravity vector and requires that the landing surface be horizontal. A disadvantage of the JPL and Hughes studies is that they have not utilized soil models, but instead have described the surface in terms of its strength for a Surveyor footpad.

1.2 Simulation Procedures

In this section a brief resume of the techniques used in the computer simulation will be given. There are three separate topics to be considered: the soil model, the spacecraft model including a description of the shock absorber model (both old and new shock absorbers), and the simulation procedure itself. The reader will be referred elsewhere for more complete information than is given in this section.

The soil model which has been used in these simulations represents the behavior of an incompressible material such as sand. The flow pattern of the soil is shown in Figure 1. The calculation of the force resisting the penetration of the footpad includes the dynamic effects arising from the acceleration of the mass of soil in the flow pattern.

The soil is described in terms of an internal friction angle ϕ , a density ρ , and a cohesion c . Chandeysson⁽⁵⁾ has given a more complete description of the soil model. Tables which relate the internal friction angle, the density and the cohesion to bearing capacity and dynamic forces for both a Surveyor and a LM sized footpad are given in Reference 1.

The spacecraft itself is divided into three parts: the main spaceframe, the landing leg assembly (including the shock absorber) and the footpad. Both the landing leg assembly and the footpad are taken to be massless in the simulation. A schematic diagram of a landing leg assembly is shown in Figure 2. There are three landing legs located at equal angles about the spaceframe.

We consider only landings in which the velocity of the spacecraft is vertical, the footpads touch simultaneously on a horizontal surface, and the surface material is the same under each footpad. In this circumstance, we need follow the motion of only a single shock absorber and landing leg, since all three behave identically. Because of the orientation of the spacecraft velocity and attitude relative to the surface, we will refer to the simulation as one dimensional, although the geometry of the landing gear is correctly taken into account. Reference to Figure 2 will show that this is inherently two dimensional.

The soil model itself is based upon the assumption that the footpad penetrates vertically into the surface. Such motion is in general not possible because the stroking motion of the landing gear alters the distance between the footpad and the spaceframe. However, if the spacecraft

descends vertically, the horizontal motion of the footpad has a maximum range of two inches. In comparison, the bottom of the footpad has a diameter of 8 inches. Thus if the spacecraft itself has no horizontal velocity, the horizontal motion of the footpad is of such limited extent that the motion would not be expected to alter the flow pattern that is the basis of the soil model.

The soil model provides information only about the vertical force exerted on the footpad. There is in addition the possibility that the soil exerts horizontal forces on the footpad. Such forces arise because of friction and, where the footpad has penetrated the surface, because the footpad must plow through the soil. No model has yet been developed to describe the horizontal forces in terms of the soil interaction. Most of the simulations were made with the assumption that no horizontal forces were exerted on the footpad. The deviations to be expected from the results due to the presence of horizontal forces were estimated by calculating the force as if it were due to ordinary friction with an arbitrarily assigned coefficient of friction. It has already been shown⁽¹⁾ that horizontal forces do not significantly affect the footpad penetration data in the range of interest to Surveyor.

The force exerted by the footpad on the spacecraft is moderated by the shock absorber. The force in the shock absorber, which is the force measured by the strain gage, depends only on the distance the shock absorber has stroked (the spring force) and the stroke rate (the damping force). The model of the new shock absorber includes a friction force which changes discontinuously when the stroke rate changes sign.

The damping force is the product of a damping coefficient times the square of the stroke rate, and is directed opposite to the motion. The damping coefficient varies with the stroke, and is shown in Figure 3 for both the old and new shock absorber. The spring force is illustrated in Figure 4. The forces given in the figures refer to forces in the shock absorber itself. The vertical force exerted on the spacecraft, which determines the acceleration along the direction of motion, must be determined from the shock absorber force with regard to the instantaneous geometry of the landing gear assembly.

In addition, the spacecraft interacts with the surface through crush blocks which are located beneath each landing leg (see Figure 2). This interaction is taken into account in the simulations.

There are two modes of calculation in the simulation. When the force levels are below the pre-load force of the shock absorber at their zero stroke position, the spacecraft behaves as a rigid body, and we will speak of the rigid mode. In other circumstances, the force exerted on the spacecraft is determined by the stroke and stroke rate of the shock absorber; this is termed the active mode.

The calculations proceed in the following way. At any given time, the position and velocity of both the spaceframe and the footpads are known. Through the use of the soil model and the shock absorber model, the relevant forces and accelerations can be determined at the particular time. It is assumed that these remain constant for a short period of time, here taken to be .0002 seconds, and the condition of the spacecraft at the end of the interval can be determined. The process is repeated until the significant motion of the spacecraft is completed.

Reference 1 contains a more complete discussion of the simulation procedure and of the behavior of the old shock absorber. Reference 2 describes in more detail the characteristics of the new shock absorber.

The spacecraft parameters used in the simulation are listed in Table I. They have been chosen to correspond to the landing conditions of Surveyor I. The landing of Surveyor I corresponded closely to the simplifying assumptions about attitude, velocity and surface slope upon which this study is based. Subsequent Surveyors have had more complicated landings and the results given here are applicable to those missions only in a general sense.

In any event, the only parameters entering into the simulation which would vary from mission to mission are the vertical velocity at touchdown and, to a lesser extent, the spacecraft mass. The sensitivity of the results to variation of the touchdown velocity will be discussed in the next section.

2.0 STRAIN GAGE TRACES

2.1 Description

The strain gage traces presented here were plotted automatically from the simulation data by the computer program. One point every .005 seconds was plotted. While this was adequate to show the overall shape of the curve of strain gage force versus time, very rapid changes, such as the oscillations which will be discussed below, may be distorted in the graph.

A computed strain gage trace for the old shock absorber is shown in Figure 5; the principal features are labeled. A similar graph for the new shock absorber is given in Figure 6.

The initial value of the strain gage force has the same value in all cases where there is no horizontal friction and where the touchdown velocity is the same. This value of the force, for the touchdown velocity used in this study, is 830 pounds for the old shock absorber and 1530 pounds for the new. The force at zero time is primarily dependent on the initial conditions assumed for the simulation, and has no dependence on the properties of the soil. The initial conditions are that the footpads are at rest (in the vertical direction) on the soil, with the spaceframe moving downward with the given initial velocity. These conditions are consistent with the assumption of negligible (or zero) mass associated with the footpads and landing gear assembly, provided also that the mass of soil in the flow pattern is non-zero.

Although the footpad is at rest in the vertical direction at time zero, horizontal motion of the footpad is required because of the stroking action of the shock absorber. In cases where horizontal friction is assumed, there is a contribution at zero time and the initial value of the strain gage force is slightly altered.

In Figure 6, the strain gage force decays from its initial value and goes through a local minimum. Both the initial value of the force and its subsequent decay are artifacts of the simulation and arise because of the particular choice of initial conditions which have been used. The presence of mass in the footpad and flexibility in the landing leg members, as well as the obviously finite frequency response of the strain gage itself, would lead to an initial recorded force level of zero. The strain gage force which would probably be observed from a real shock absorber is shown as a dotted line in Figure 6.

In the case of the new shock absorber, a change in the direction of stroking of the shock absorber produces a discontinuous change in the strain gage force because the friction force changes sign when the stroke rate does. A similar discontinuity does not occur for the old shock absorber since no frictional forces were included in that model.

The discontinuous change in the strain gage force is readily apparent in Figure 6. As may be seen in this Figure a period of oscillation occurs in the simulation. The shock

absorber motion varies between positive and negative stroke rates, and this results in a series of discontinuous changes in the force. Since only every twenty-fifth computed point is plotted, the graphs do not in general represent an accurate picture of the oscillation, and in most figures such regions of oscillation will be replaced by cross-hatching.

The oscillations do not occur in all cases, but only when the footpads are still penetrating through the soil at the time when the relative velocity between the spaceframe and the footpads approaches zero. The oscillation terminates as soon as the footpads come to rest. The phenomenon arises because the discontinuous change in the shock absorber force is sufficient to alter the trend of the relative motion between the footpad and spaceframe.

The oscillation is not a defect, but rather an artifact of the simulation. For the actual spacecraft, the flexibility of the landing leg, the mass of the landing gear assembly and the true behavior of the frictional force would act to remove the discontinuous change in the force.

At this point, we are prepared to study the effect on the strain gage traces caused by the introduction of horizontal forces at the footpad. The effect is shown for the old shock absorber in Figures 7, 8 and 9. Figure 7 is for a very strong soil, which is not penetrated by either the Surveyor footpad or crush block. Figure 8 is a soil chosen to be consistent with Surveyor I penetration data,⁽¹⁾ and Figure 9 is for a weaker soil which allows a Surveyor footpad penetration of about 1 foot. The parameters of the soil model used in these simulation are indicated on the figures.

Corresponding curves are shown for the new shock absorber in Figure 10 for the strong soil, in Figure 11 for the moderate strength soil, and in Figure 12 for the weak soil.

The horizontal forces are calculated using a coefficient of friction; that is, the horizontal forces are taken to be proportional to the vertical footpad force with a constant of proportionality given by the coefficient of friction. It is not suggested here that this is an adequate representation of the actual forces; rather, the use of a coefficient of friction is only a convenient way to generate horizontal forces of various magnitudes in order to explore their effect on the strain gage trace.

It may be seen in Figures 7 through 12 that horizontal forces of a magnitude equal to the vertical forces ($\mu = 1$) do indeed significantly alter the quantitative values of the strain

gage trace while not affecting the overall shape of the curve to a large extent. This is unfortunate because, as we shall see in the next section, these changes are similar to those produced by a variation of the soil parameters. There is no apparent way to separate effects produced by horizontal forces from those which discriminate between soils of different properties.

2.2 Results

In this section, typical strain gage traces for a variety of soil conditions will be presented, and a comparison made with the data obtained from Surveyor I. We will then consider briefly the problem of interpretation of strain gage traces.

Figure 13 illustrates the variation of the strain gage trace as a function of the bearing capacity of the soil in the case of the old shock absorber. The internal friction angle of the soil is 30° and the density is 3 slugs/ft^3 ; the cohesion is varied to adjust the bearing capacity. The curves are given for the same soil parameters but for the new shock absorber in Figure 14. The significant feature of these curves is the general trend that as the bearing strength increases, the maximum force of the strain gage trace increases and its time duration decreases.

In previous work, the depth of penetration observed in the landing of Surveyor I was used to select sets of soil parameters. These sets are listed in Table II. Clearly a continuum of such sets of parameters is possible, but the sets listed in Table II will be taken as a representative sample of potential lunar soils. It is interesting to determine the extent to which the strain gage trace data could be used to discriminate among these sets. This is done for the old shock absorber (Surveyor I) in Figure 15 for a soil density of 1 slug/ft^3 , and in Figure 16 for a soil density of 3 slugs/ft^3 . Strain gage traces for those sets of soil parameters listed in Table II but not given in the figure are very nearly identical (for both densities) to the curves for the internal friction angle of 0° .

Comparison of the two figures reveals that there exists at most a small difference among the traces for various sets of soil parameters. These data provide no basis for using strain gage traces to seek details of the lunar soil parameters for the conditions modeled here.

Similar curves for the new shock absorber are shown in Figures 17 and 18. While the simulated data shows greater differences, compared to that for the old shock absorber, the differences do not appear to be of adequate degree to serve as a discriminant among the sets of soil parameters given in Table II.

There is another way to study this topic. It may be seen that all the strain gage traces have the same general shape. Apart from detailed structure, which we will ignore, they rise to a simple maximum and then decay. Let us take the maximum of a trace as the sole measure of the trace. It has already been noted that the time duration of the trace increases as the maximum of the force decreases, so that it is not unreasonable to assume that the maximum force contains most of the information available in a given trace. This assumption will have greater validity in the presence of noise, as in the case of the actual data, since noise will obscure much of the detailed shape of the strain gage trace. Even if the details of the actual traces were accessible, it would not be realistic to expect the simulation to reproduce them since the simulation uses only a very simplified model of the spacecraft.

Care must be exercised in extracting the maximum in certain circumstances. As we explained previously, the initial value of the strain gage force is fixed by the initial conditions and is therefore somewhat arbitrary. In some cases, especially for soils with low bearing capacity, the initial value is the maximum strain gage force. However, the desired maximum is the local maximum which occurs subsequently (see, for example, the curves in Figure 9).

The peak strain gage force for various values of the internal friction angle is plotted as a function of the surface static bearing capacity in Figure 19 for the old shock absorber and in Figure 20 for the new. The bearing capacity scale is specific to the Surveyor footpad; the bearing capacity is derived from the soil parameters but depends on the dimension of the penetrating object.

These curves illustrate the sensitivity of the strain gage trace to both the bearing strength of the soil and to the internal friction angle. For soils having a bearing capacity of greater than about 10 psi (specifically 9.8 psi for the old and 9.6 psi for the new shock absorber), the maximum pressure level at the footpad is less than the surface bearing strength of the soil and no footpad penetration occurs. The crush blocks, on the other hand, exert a maximum pressure of 40 psi and so penetrate any soil having a smaller bearing capacity. Between 10 and 40 psi, changes in the soil bearing capacity produce subtle changes in the decay of the

strain gage trace. However, these changes do not alter the maximum of the strain gage trace as is apparent in Figures 19 and 20.

If the surface bearing capacity of the soil has been measured by some other technique, such as a determination of the footpad penetration, and it is less than 10 psi, it is conceptually possible in some circumstances to obtain a value for the internal friction angle through a determination of the maximum strain gage force, if the horizontal forces may be neglected as they have been in the simulation. It is well to consider how the preceeding information is altered by the presence of horizontal forces at the footpad. This is done in Figure 21 and 22 for the old and new shock absorber, respectively. It is immediately clear that the presence of horizontal forces equal in magnitude to the vertical forces will significantly change the maximum strain gage force, and mask any sensitivity to the internal friction angle of the soil. Unfortunately, the spacecraft data do not provide an indication of the value of the horizontal forces. It must be left to intuition to decide whether a coefficient of friction of unity provides a low, reasonable or excessive estimate of the actual horizontal forces. The important conclusion is, however, that the strain gage maximum can be appreciably affected by horizontal forces which are not so large as to be inconceivable.

Consequently, it appears that the strain gage data cannot be used to further our understanding of the soil properties. This result arises from a lack of knowledge of the horizontal forces on the footpad. A realistic model of the horizontal forces would be of great value in extending the usefulness of the strain gage data.

The details of the strain gage traces, and specifically the maximum strain gage force, vary with the touchdown velocity of the spacecraft. The variation of the maximum force is shown in Figure 23. The touchdown velocity varied from mission to mission. A value of 11.7 ft/sec, corresponding to the result from Surveyor I, has been used on the remainder of the simulations.

We are now prepared to compare the simulated strain gage traces for the old shock absorbers with the data from Surveyor. The landings of Surveyors III and V were asymmetric; that is, the different landing legs on each spacecraft impacted and stroked in an individual manner. Since symmetry is an important assumption of this study, detailed consideration of those data is not possible in this study. Surveyors VI and VII were flown after the simulations reported here were completed.

The original data from Surveyor I are shown in Figure 24. Leg 3 has not been included because of the calibration uncertainty for that leg.⁽³⁾ The maximum strain gage force is approximately 1400 pounds for leg 1 and 1600 pounds for leg 2. Comparison of these numbers with the results presented in Figure 19 shows that these data are consistent with a bearing strength of between 6 and 8 psi and an internal friction angle between 0° and 40°, if horizontal forces are neglected.

A comparison between the observed and simulated strain gage data is given in Figure 25 for leg 1. The curve for the observed data has been highly smoothed from the original data, which contained considerable noise, and the curve has been translated in time to obtain the best fit. It is apparent that the simulated strain gage force does not decay as rapidly as the actual force. A better overall fit is obtained with harder surfaces, although this is accomplished at the expense of disagreement with the peak force levels.

All of the comparisons with the Surveyor I data have been carried out at a soil density of 3 slugs/ft³, which is suggested by Scott and Roberson⁽⁶⁾ on the basis of a preliminary analysis of data from the Surveyor III Soil Mechanics Surface Sampler Experiment. They also suggest an internal friction angle of 39° and a cohesion of .02 psi; this corresponds to a surface bearing capacity for a Surveyor footpad of about 5.5 psi. The estimates obtained from comparison of the strain gage data from Surveyor I with the simulated results are in agreement with the estimates of Scott and Roberson, and with the estimate of 6 psi for the surface bearing capacity⁽¹⁾ obtained by comparison of simulated landings with the footpad penetration data of Surveyor I.

3.0 STRAIN GAGE FILTER

The strain gage traces obtained from the Surveyor spacecraft represent not the actual force levels in the strain gage, but the force level time history as modified by a series of elements each of which alters the signal in some fashion. The strain gage itself is not a perfect transducer, and every element in the transmission and reception system imposes its characteristic response on the observed traces. In this section we will estimate the effect of the filters on the observed signals.

For the Surveyor strain gage system,⁽⁷⁾ the limiting filter is at the Deep Space Net receiving station. That is, other filters in the system are significantly less restrictive than at the receiving station, and the net effect of all of the filters in the system is approximately the same as that due to the filter at the receiver. A restrictive filter is required at this point in order to improve the signal-to-noise ratio.

In what follows, then, we will consider only a single filter which is characterized by a single parameter, the cutoff frequency, which is the point at which the frequency response has fallen by 3 db relative to its response to a d.c. signal. The frequency response $J(f)$ in db is given by

$$J(f) = 20 \log_{10} A(f) \quad (1)$$

where $A(f)$ is the amplitude response to a unit amplitude sine wave input of frequency f . The cutoff frequency f_0 is the frequency at which $J(f)$ is equal to -3db.

The filter used for the strain gage channel at the Deep Space Net receiving station during the Surveyor I mission was a 6th order Butterworth filter with a cutoff frequency of 56 Hz.⁽⁷⁾ We will assume that this filter represents the response of the system. The 3 db frequency f_0 may change from mission to mission within the Surveyor Program depending on the precise requirement of the overall telemetry system. To allow the results of this section to be extended to cases where the cutoff frequency is other than 56 Hz, we will also study the strain gage traces as they appear after passing through a 6th order Butterworth filter having a cutoff frequency of 20 Hz. In addition, we will consider certain properties of the filter parametrically with frequency. However, this study is based solely on the use of a 6th order Butterworth filter, and should the assumption about the relative importance of the filters or about their type change, the entire problem must be reconsidered.

A Butterworth filter, which is also called a maximally flat low-pass filter, is defined to possess the following frequency response⁽⁸⁾

$$A(f) = \frac{1}{\left[1 + \left(\frac{f}{f_0}\right)^{2n}\right]^{1/2}} \quad (2)$$

where A is the amplitude response at frequency f , n is the order of the filter and f_0 is the cutoff frequency. The transfer function and the impulse response function of a 6th order Butterworth filter are tabulated in Table III; the impulse response function is shown in Figure 26.

The filtered strain gage signal $R(t)$ is obtained from the input signal $r(t)$ through the relation

$$R(t) = \int_{-\infty}^t r(\tau) i(t-\tau) d\tau \quad (3)$$

where $i(t')$ is the impulse response at time t' after the impulse. The integral is solved in the computer program by using a step function approximation to the curves $r(t)$ and $i(t)$.

Figures 27 through 30 show typical filtered strain gage outputs in comparison with the original signal. Figures 27 and 28 show the old and the new shock absorber, respectively, at a cutoff frequency of 56 Hz. The curves are repeated in Figures 29 and 30 for a cutoff frequency of 20 Hz.

An obvious effect of the filter on the strain gage trace is the reduction of the initial value of the trace ($t=0$) to zero. This clearly arises from the limited passband of the filter. In addition, however, there are two important effects which we will consider in greater detail: the overshoot and the delay. In order to facilitate the discussion, we will determine the effect of the filter on a very simple waveform. From this it is then possible to achieve a qualitative understanding of the effect of the filter on a more complicated input waveform.

The standard waveform and the effects which we will consider are illustrated in Figure 31. It consists simply of a linear ramp which rises to unit value in a time τ (the rise time), after which it maintains a plateau value at unit amplitude.

The response of the filter to the standard input signals is shown in Figure 32 for several values of the rise time. It is clear that the filter produces a distinct overshoot and that the overshoot decreases as the rise time increases. The overshoot is presented as a function of the rise time in Figure 33. For a cutoff frequency of 56 Hz, only a small overshoot results for a rise time greater than .02 seconds.

The second feature which is apparent in Figure 31 is the delay. It may be shown from analysis of the transfer function for the Butterworth filter that an input signal which is linear with time produces an output signal which has the same shape but which is delayed by an amount

$$t_D = .615/f_0 \quad (4)$$

if one disregards the transients associated with the initiation of the signal. The transients have a decay constant greater than $\pi f_0/2$, so that they are important only for about $1/f_0$ seconds following an abrupt change in the signal.

In the case of Surveyor I, if the input signal is approximated by a linear rising signal, the output signal received at earth would also be a linearly rising signal delayed by 11 milliseconds. The first .02 seconds following the start of the input signal would be dominated by the transients.

The implication of this information on the interpretation of the strain gage traces from Surveyor I is clear. The first 20 milliseconds of signal show the characteristics of the filter, not of the actual strain gage signal. The signal as received is delayed approximately 11 milliseconds; the delay is appropriate to linear sections of the input signal. These results are shown clearly in Figure 28.

If the cutoff frequency of the filter is altered, the qualitative effect of the filter is unchanged as long as the type of filter remains the same. However, the quantitative value of the effects will change. The cutoff frequency has been retained in all the relations in order that the appropriate values may be easily calculated.

With reference to Figures 29 and 30, it may be seen that even with a cutoff frequency as low as 20 Hz, the general shape of the strain gage trace is not affected by the presence of the filter. Of course the same statement is true at a cutoff frequency of 56 Hz. Even the presence of the overshoot arising from the filter does not alter in any sensible way the maximum value of the strain gage force. The bumps produced by the filter are of no greater magnitude than the fine structure of the simulated strain gage traces. Moreover, the presence of noise in the received signal (see Figure 24) obscures not only the detailed structure of the strain gage trace itself, but also any fine structure arising from the filter.

Consequently we arrive at the conclusion that the presence of filters, as specified, in the telemetry channels used for the Surveyor strain gage data does not materially affect the interpretation of the data. Foreknowledge of this conclusion enables us to discuss the interpretation of the data before including the additional complication of the filter in the strain gage channel. However, the delay produced by the presence of the filter may be of sufficient magnitude to warrant consideration in detailed studies of the timing of the sequence of events in the touchdown phase of Surveyor landings.

4.0 CONCLUSIONS

The purpose of the memorandum has been to explore the interpretation of strain gage traces obtained during the landing of a Surveyor spacecraft in terms of establishing detailed characteristics of a soil model for the lunar surface. The use of a soil model in describing the interaction between a spacecraft and the lunar surface is essential if it is desired to extend the observations to the prediction of results for spacecraft having different footpad dimensions.

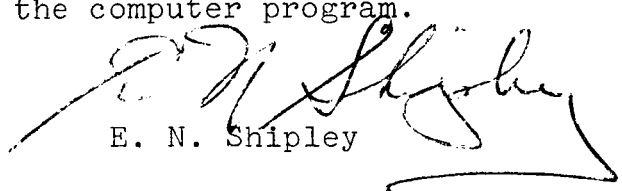
The principal results which have been obtained are:

- 1) because of the lack of knowledge about the horizontal forces acting on the footpad, it is not possible to obtain detailed soil characteristics from the strain gage traces, and
- 2) filters which exist in the strain gage data telemetry channel do not produce any sensible change in the interpretation of the data.

ACKNOWLEDGEMENT

Mrs. C. A. Friend contributed to this work through her efforts in modifying the computer program.

1014-ENS-ulg



E. N. Shipley

ATTACHMENTS

Tables I, II, and III
Figures 1-33

BELLCOMM. INC.

REFERENCES

1. E. N. Shipley, "Surveyor and LM Penetration in a Model Lunar Soil", Bellcomm Technical Memorandum TM-67-1014-1, February 23, 1967.
2. E. N. Shipley, "Surveyor Penetration in a Model Lunar Soil", Bellcomm Technical Memorandum TM-67-1014-5, September 6, 1967.
3. F. Sperling and J. Garba, "A Treatise on the Surveyor Lunar Landing Dynamics and an Evaluation of Pertinent Telemetry Data Returned by Surveyor I", JPL Technical Report 32-1035, August 15, 1967.
4. R. H. Jones, Hughes Aircraft Company, private communication.
5. P. L. Chandeysson, "Calculating Dynamic Soil Bearing Strength for Vertical Landing Spacecraft", Bellcomm Memorandum for File, December 7, 1966.
6. R. F. Scott and F. I. Roberson, "Soil Mechanics Surface Sampler: Lunar Surface Tests, Results and Analyses", Section IV, Surveyor III Mission Report, Part II, Scientific Results, JPL Technical Report 32-1177, June 1, 1967.
7. R. J. Rechter, Hughes Aircraft Company, private communication.
8. F. F. Kuo, Network Analysis and Synthesis, John Wiley & Sons, Inc., New York, 1966, 2nd ed., Section 13.3.

BELLCOMM. INC.

TABLE I

Surveyor Parameters Used in the Simulations

Spacecraft		
	Surveyor Mass (at touchdown)	20.0 slugs
	Touchdown Velocity	11.7 ft/sec
Shock Absorber		
	Spring force	see Figure 4
	Damping coefficient	see Figure 3
	Friction force	old shock absorber none
		new shock absorber
		40 pounds + .03 X (spring force)
Crush Block		
	Crushing Pressure	40 psi
	Effective Radius	.34 feet
Footpad		
	Radius	.33 feet

BELLCOMM. INC.

TABLE II

Sets of Soil Parameters Which Give
a Surveyor I Footpad Penetration
Depth of 0.25 Feet (See Reference 1)

SOIL PARAMETERS			SURFACE STATIC BEARING CAPACITY FOR A SURVEYOR FOOTPAD
INTERNAL FRICTION	DENSITY	COHESION	
0°	1 slug/ft ³	.95 psi	6.3 psi
0°	3	.95	6.3
10°	1	.55	6.4
10°	3	.54	6.4
20°	1	.30	6.3
20°	3	.30	6.3
30°	1	.12	6.2
30°	3	.11	6.1
40°	1	.038	5.9
40°	3	.015	5.1

TABLE III

Equations for a 6th Order Butterworth Filter

A. Transfer Function

$$h(s) = \sum_{j=1}^3 \frac{\omega_0 A_j}{s - \omega_0 C_j} + \frac{\omega_0 A_j^*}{s - \omega_0 C_j^*}$$

B. Impulse Response Function

$$r(t) = 2\omega_0 \sum_{j=1}^3 e^{\omega_0 a_j t} (R_j \cos \omega_0 b_j t - I_j \sin \omega_0 b_j t)$$

where

$$C_1 = e^{i(7\pi/12)} ; C_2 = e^{i(9\pi/12)} ; C_3 = e^{i(11\pi/12)}$$

$$A_1 = \frac{1}{(C_1 - C_1^*)(C_1 - C_2)(C_1 - C_2^*)(C_1 - C_3)(C_1 - C_3^*)} = .204 + i(.354)$$

$$A_2 = \frac{1}{(C_2 - C_1)(C_2 - C_1^*)(C_2 - C_2^*)(C_2 - C_3)(C_2 - C_3^*)} = -1.524$$

$$A_3 = \frac{1}{(C_3 - C_1)(C_3 - C_1^*)(C_3 - C_2)(C_3 - C_2^*)(C_3 - C_3^*)} = 1.320 - i(2.285)$$

$$a_j = \text{Re}(C_j) ; b_j = \text{Im}(C_j)$$

$$R_j = \text{Re}(A_j) ; I_j = \text{Im}(A_j)$$

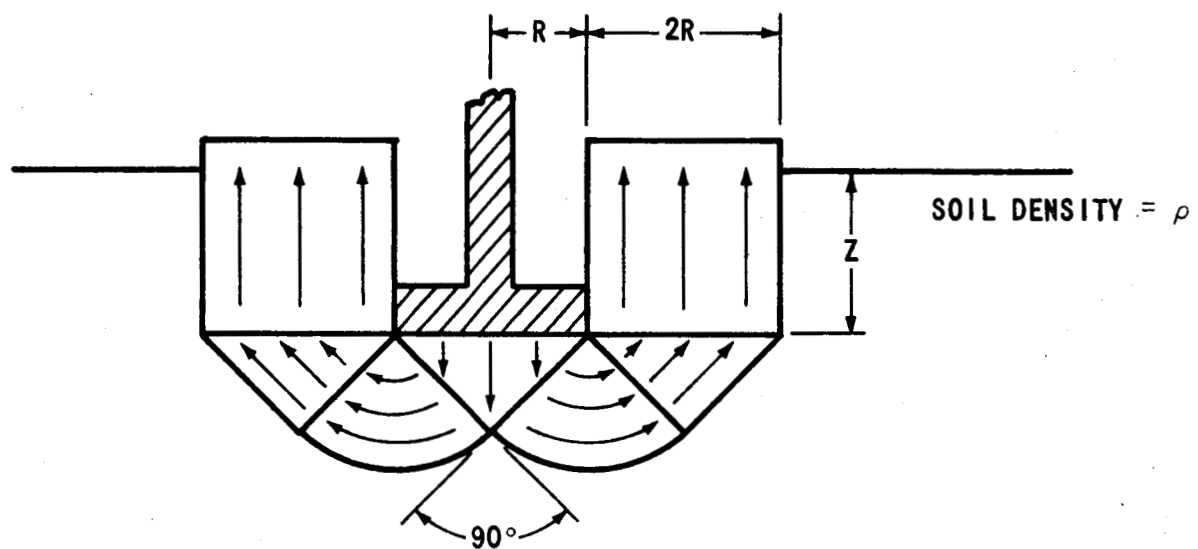
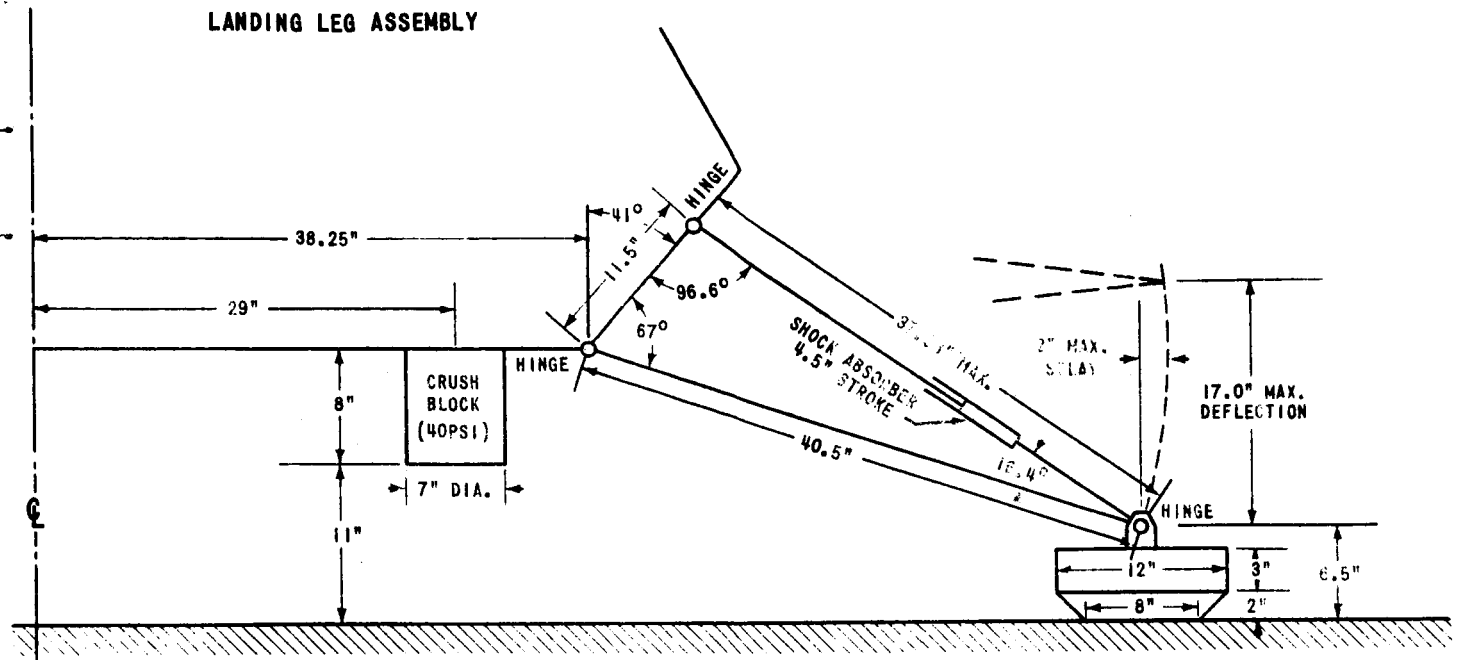


FIGURE 1 - FLOW PATTERN FOR INCOMPRESSIBLE MODEL SOIL (FROM REFERENCE 5)



FOOTPAD DETAIL

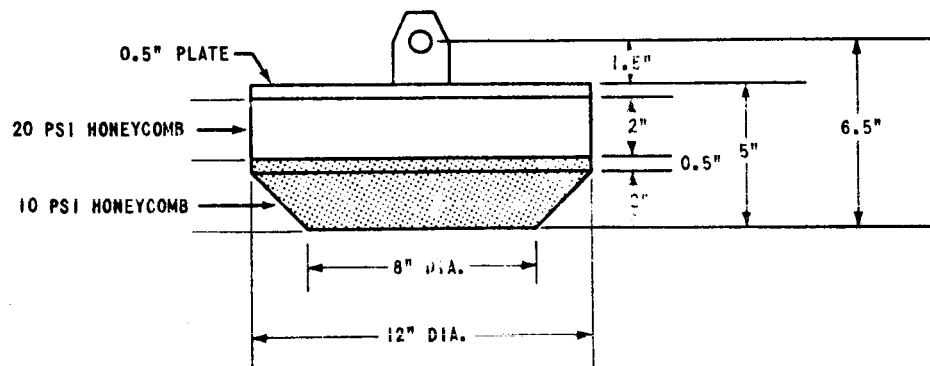


FIGURE 2 - SURVEYOR SHOCK ABSORBER GEOMETRY

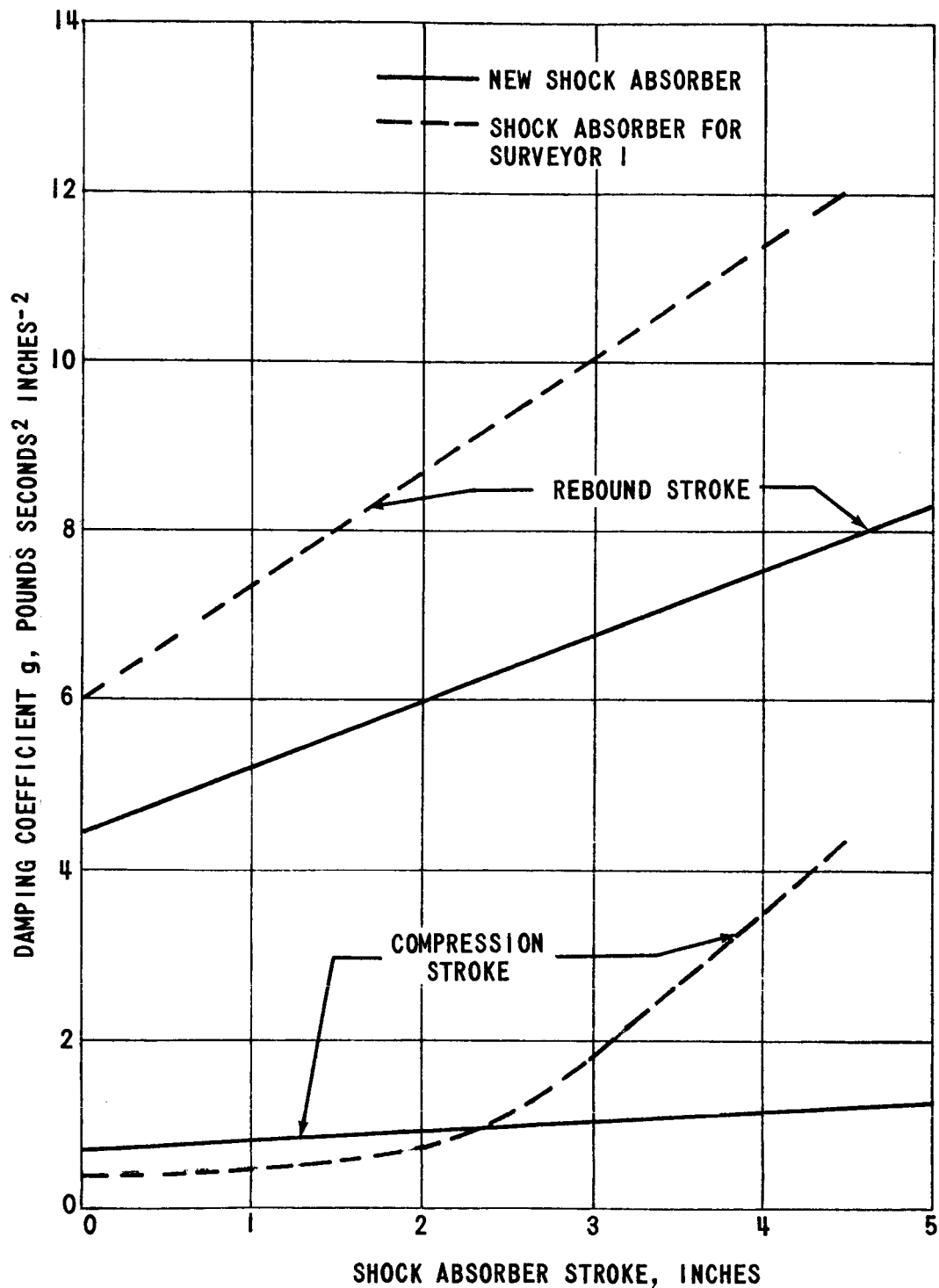


FIGURE 3 - COMPARISON OF THE DAMPING COEFFICIENT FOR THE SURVEYOR SHOCK ABSORBER. DAMPING CREATES A FORCE WHICH IS DIRECTED OPPOSITE TO THE MOTION OF THE SHOCK ABSORBER AND WHOSE MAGNITUDE IS THE PRODUCT OF THE DAMPING COEFFICIENT AND THE SQUARE OF THE SHOCK ABSORBER STROKE RATE

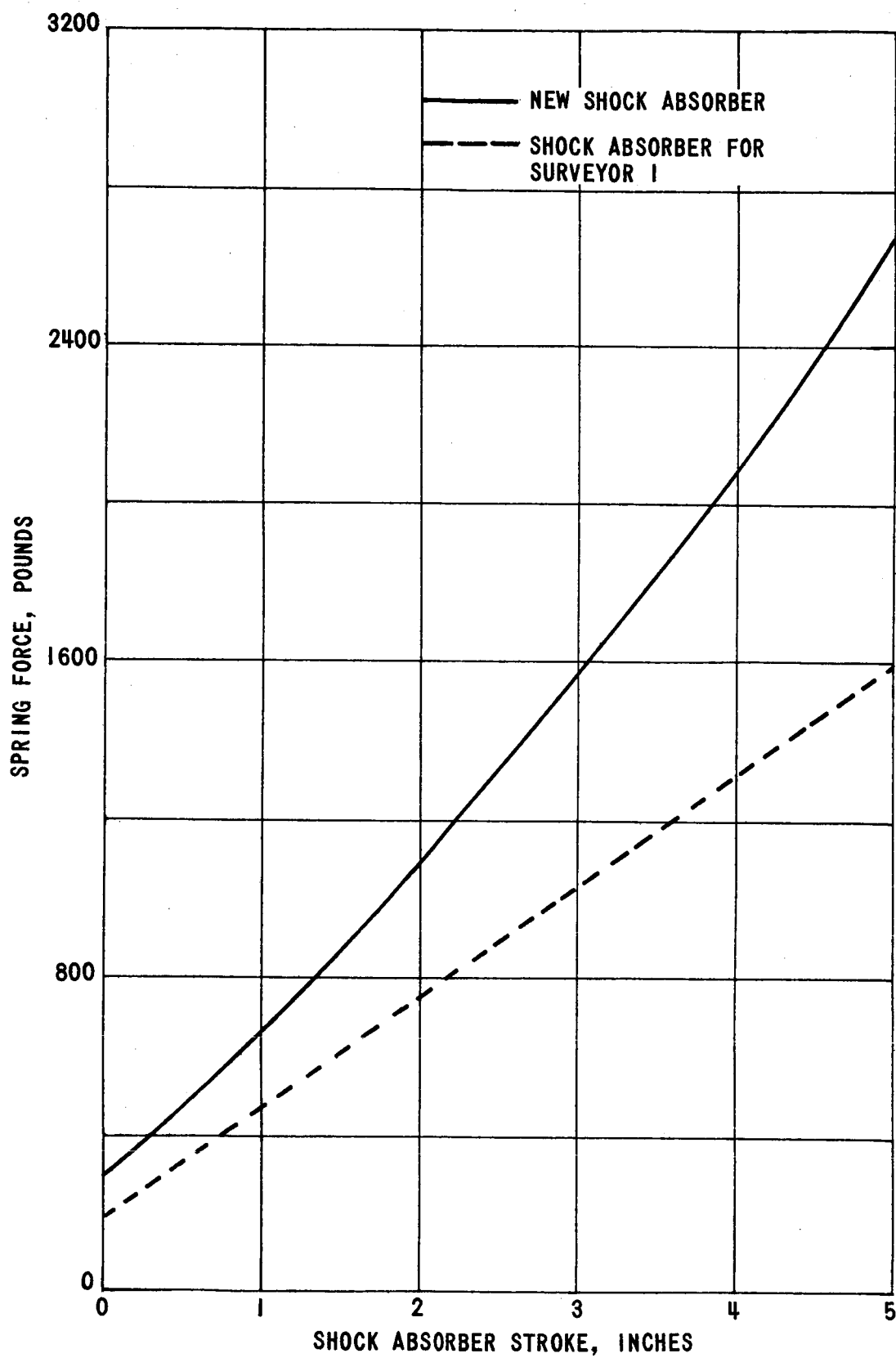


FIGURE 4 - SPRING FORCE FOR THE SURVEYOR SHOCK ABSORBER. THE GRAPHS INCLUDE THE PRELOAD FORCE

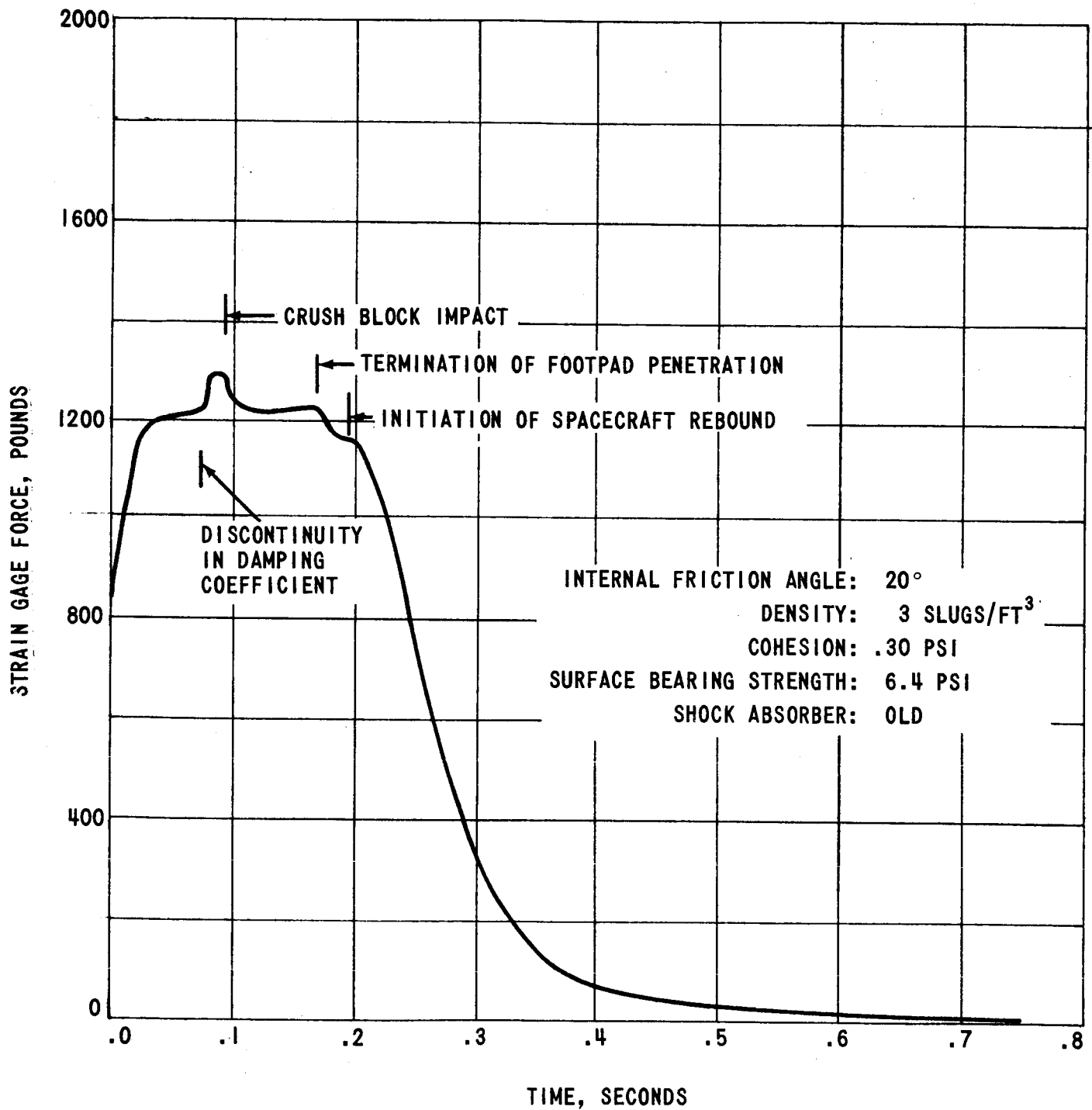


FIGURE 5 - ILLUSTRATION OF THE TIMING OF EVENTS IN THE LANDING CYCLE WHICH GIVE RISE TO THE DETAILED SHAPE OF THE STRAIN GAGE TRACE FOR THE OLD SHOCK ABSORBER

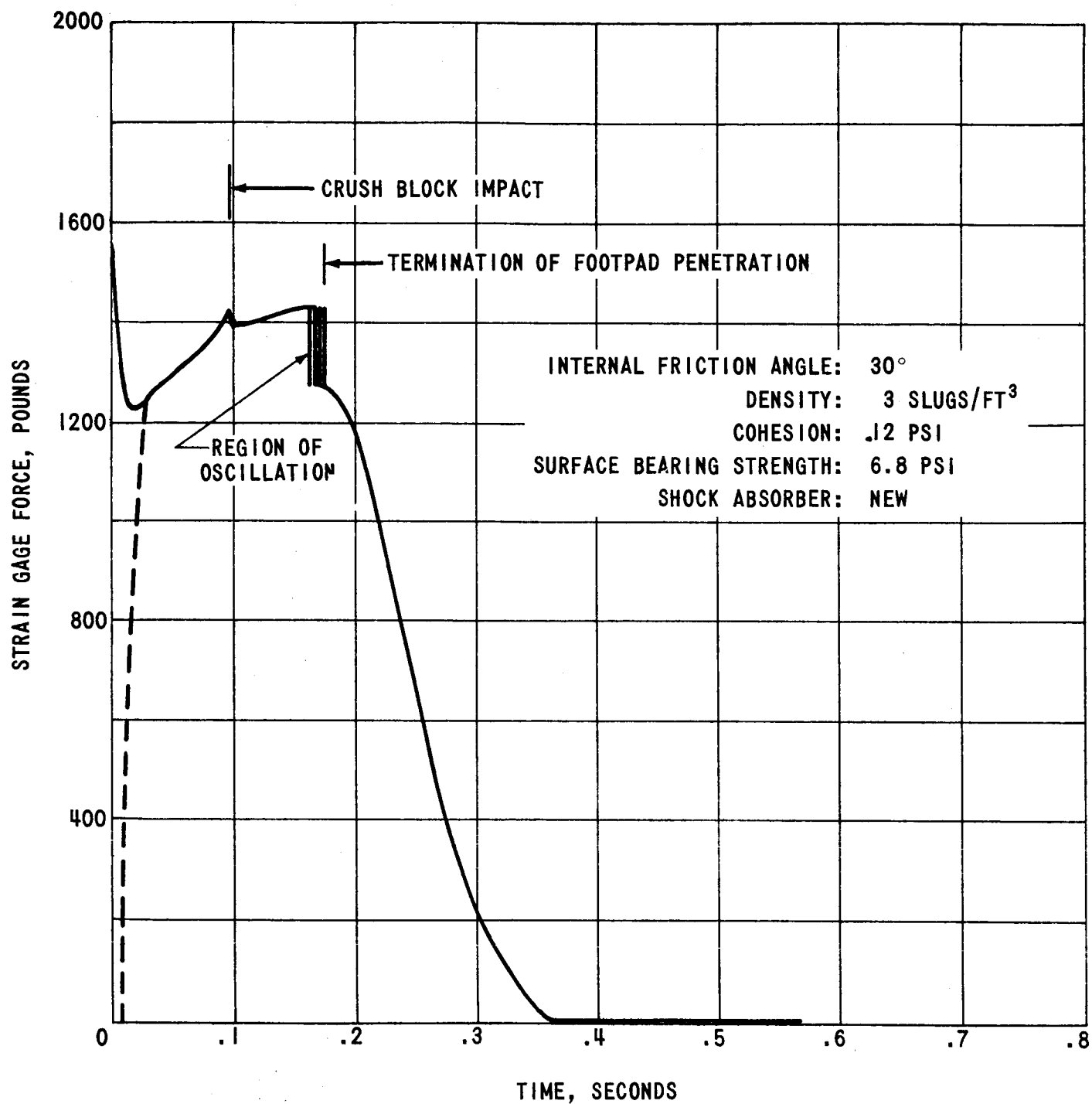


FIGURE 6 - ILLUSTRATION OF THE TIMING OF EVENTS IN THE LANDING CYCLE WHICH GIVE RISE TO THE DETAILED SHAPE OF THE STRAIN GAGE TRACE FOR THE NEW SHOCK ABSORBER. THE DASHED LINE INDICATES THE PROBABLE TRACE FOR AN ACTUAL SPACECRAFT

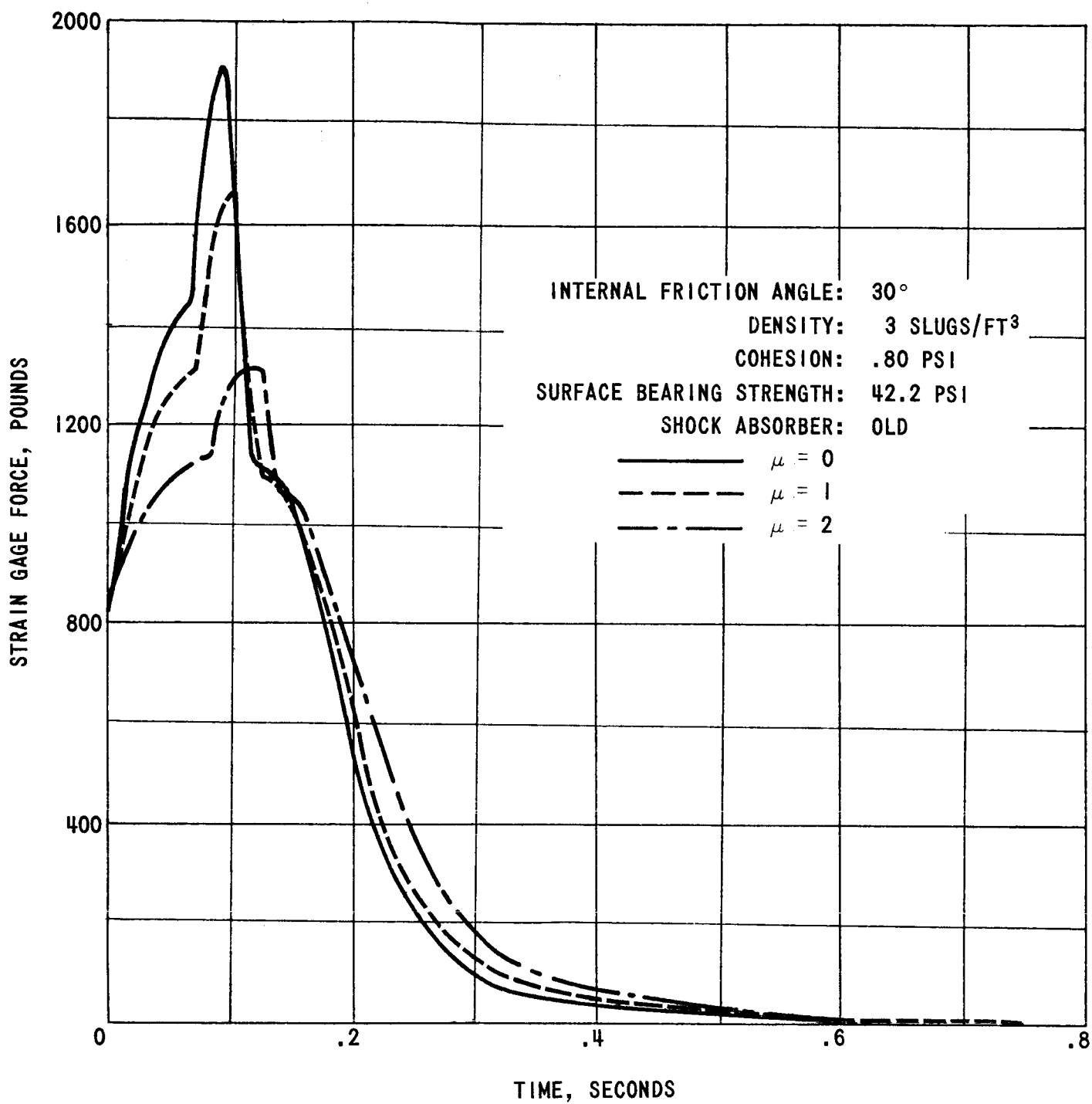


FIGURE 7 - VARIATION OF THE STRAIN GAGE TRACE DUE TO HORIZONTAL FORCES AT THE FOOTPAD. μ IS THE COEFFICIENT OF FRICTION

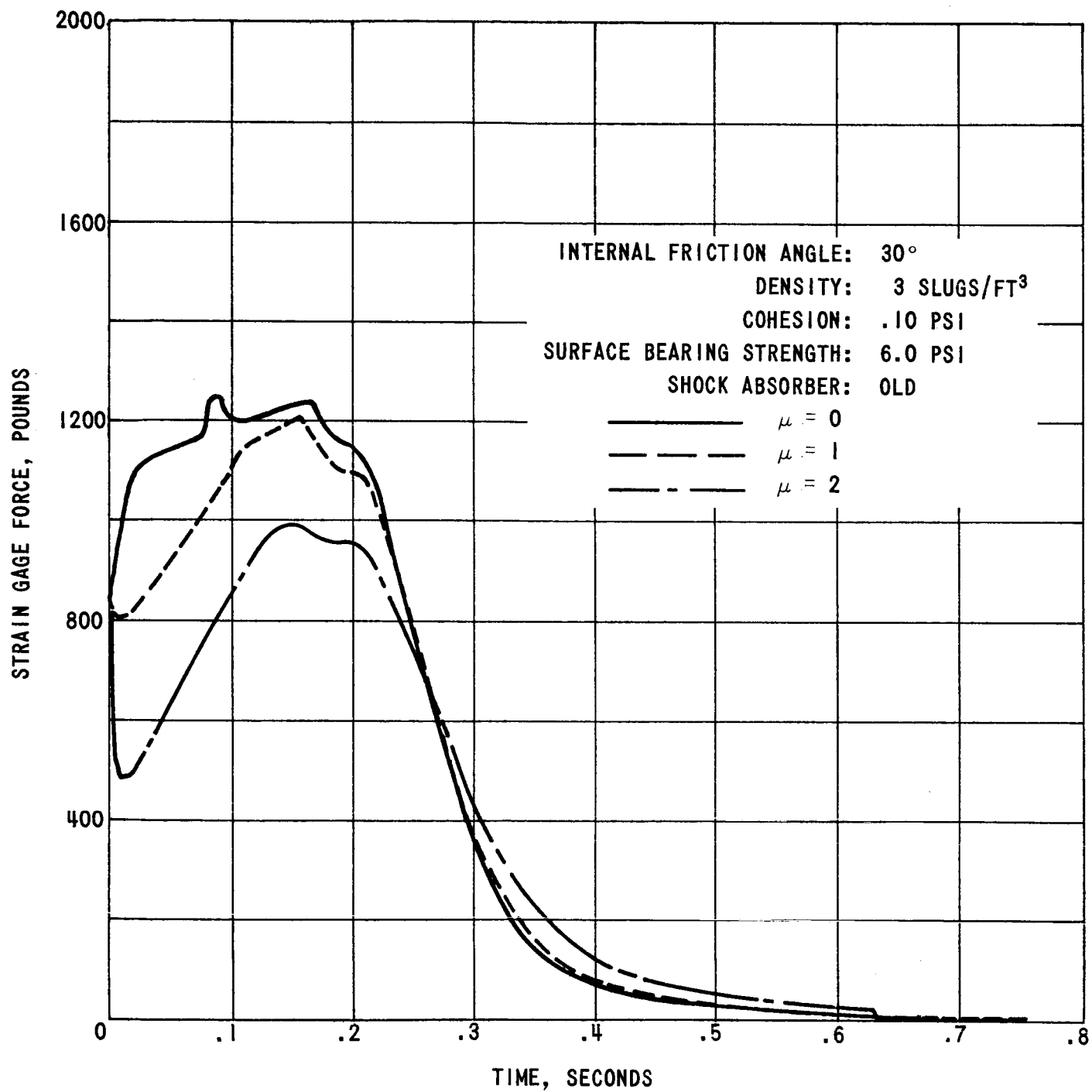


FIGURE 8 - VARIATION OF THE STRAIN GAGE TRACE DUE TO HORIZONTAL FORCES AT THE FOOTPAD. μ IS THE COEFFICIENT OF FRICTION

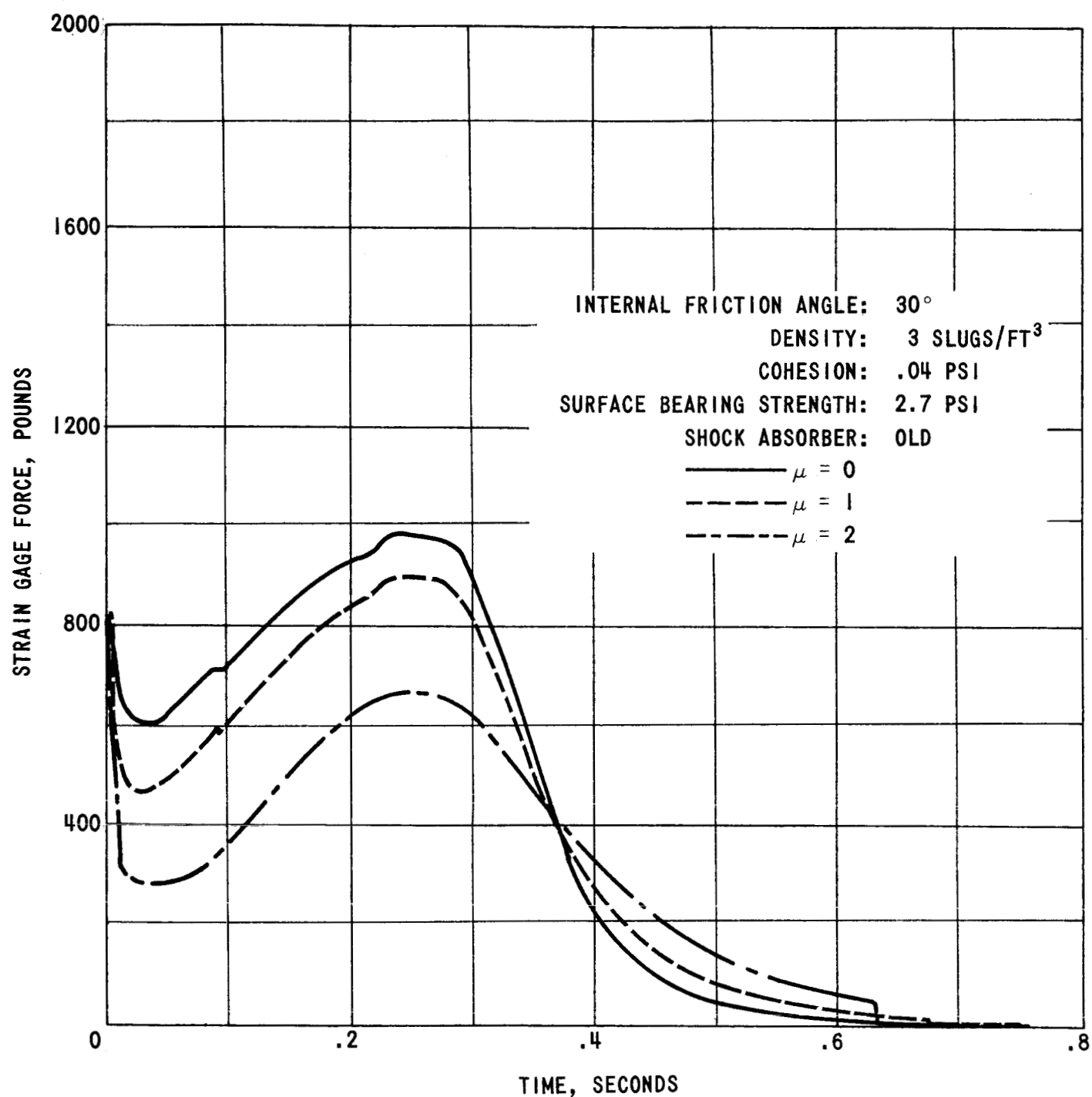


FIGURE 9 - VARIATION OF THE STRAIN GAGE TRACE DUE TO HORIZONTAL FORCES AT THE FOOTPAD. μ IS THE COEFFICIENT OF FRICTION

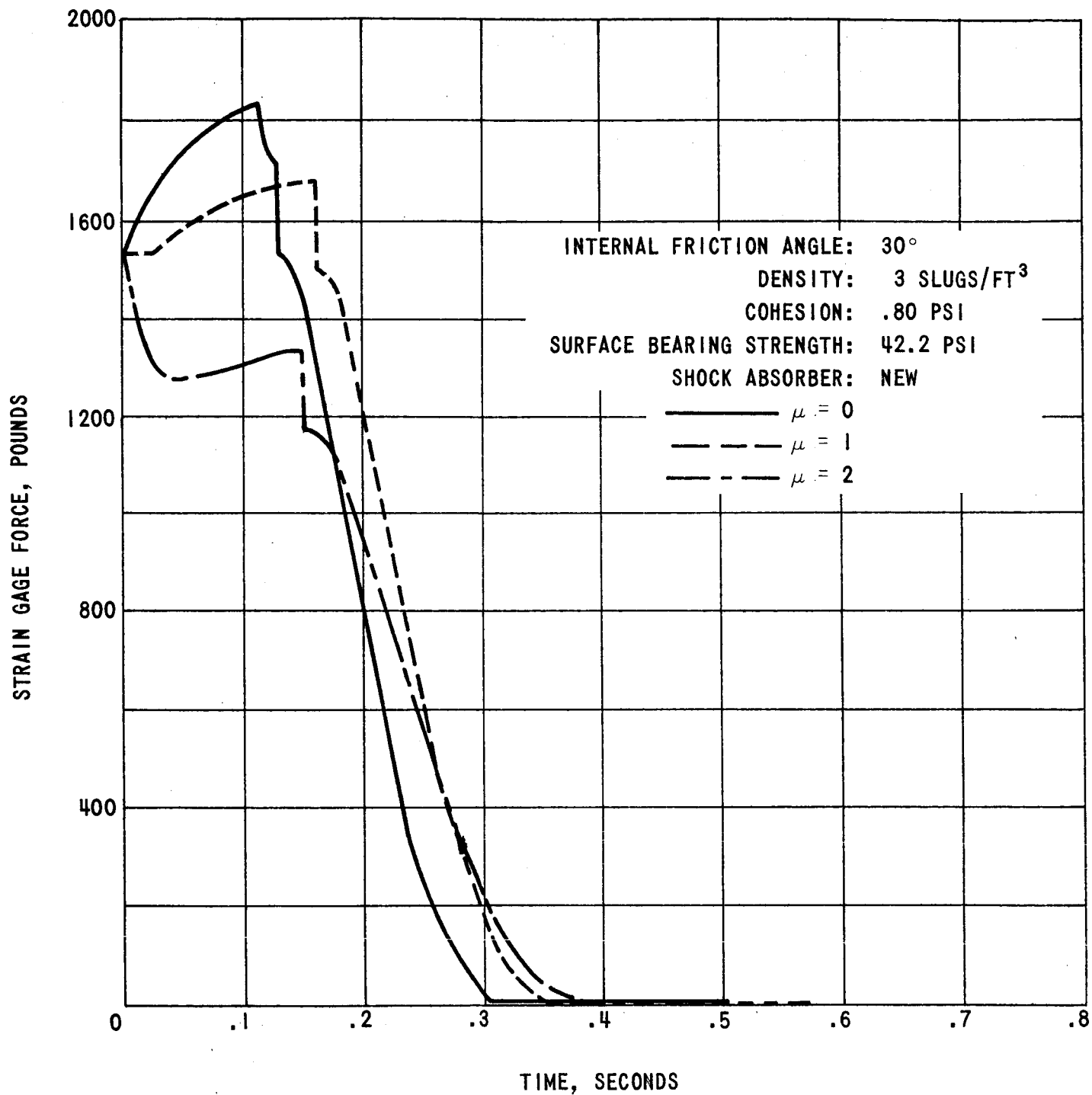


FIGURE 10 - VARIATION OF THE STRAIN GAGE TRACE DUE TO HORIZONTAL FORCES AT THE FOOTPAD. μ IS THE COEFFICIENT OF FRICTION

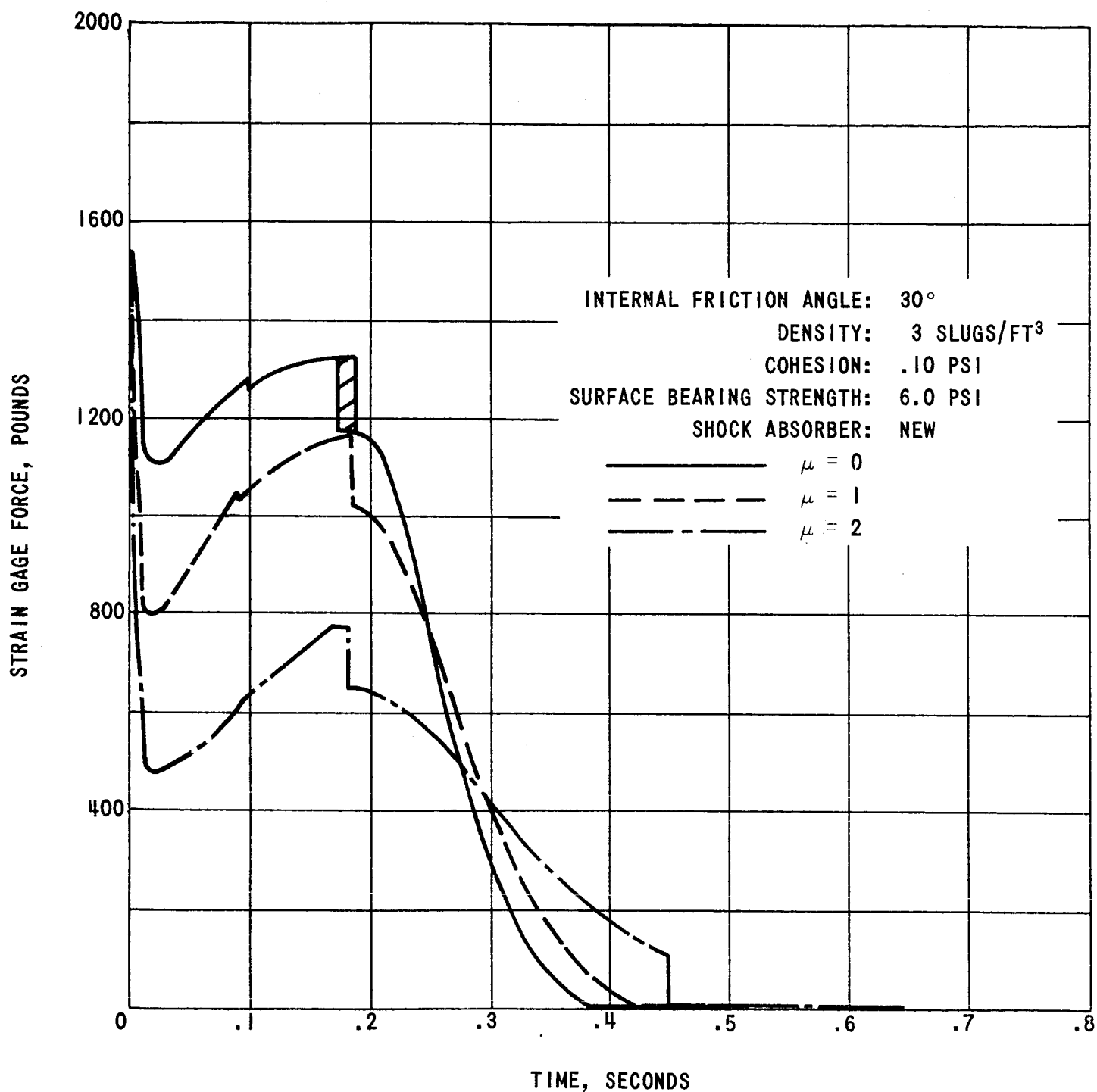


FIGURE 11 - VARIATION OF THE STRAIN GAGE TRACE DUE TO HORIZONTAL FORCES AT THE FOOTPAD. μ IS THE COEFFICIENT OF FRICTION. THE CROSS-HATCHING INDICATES A REGION OF OSCILLATION

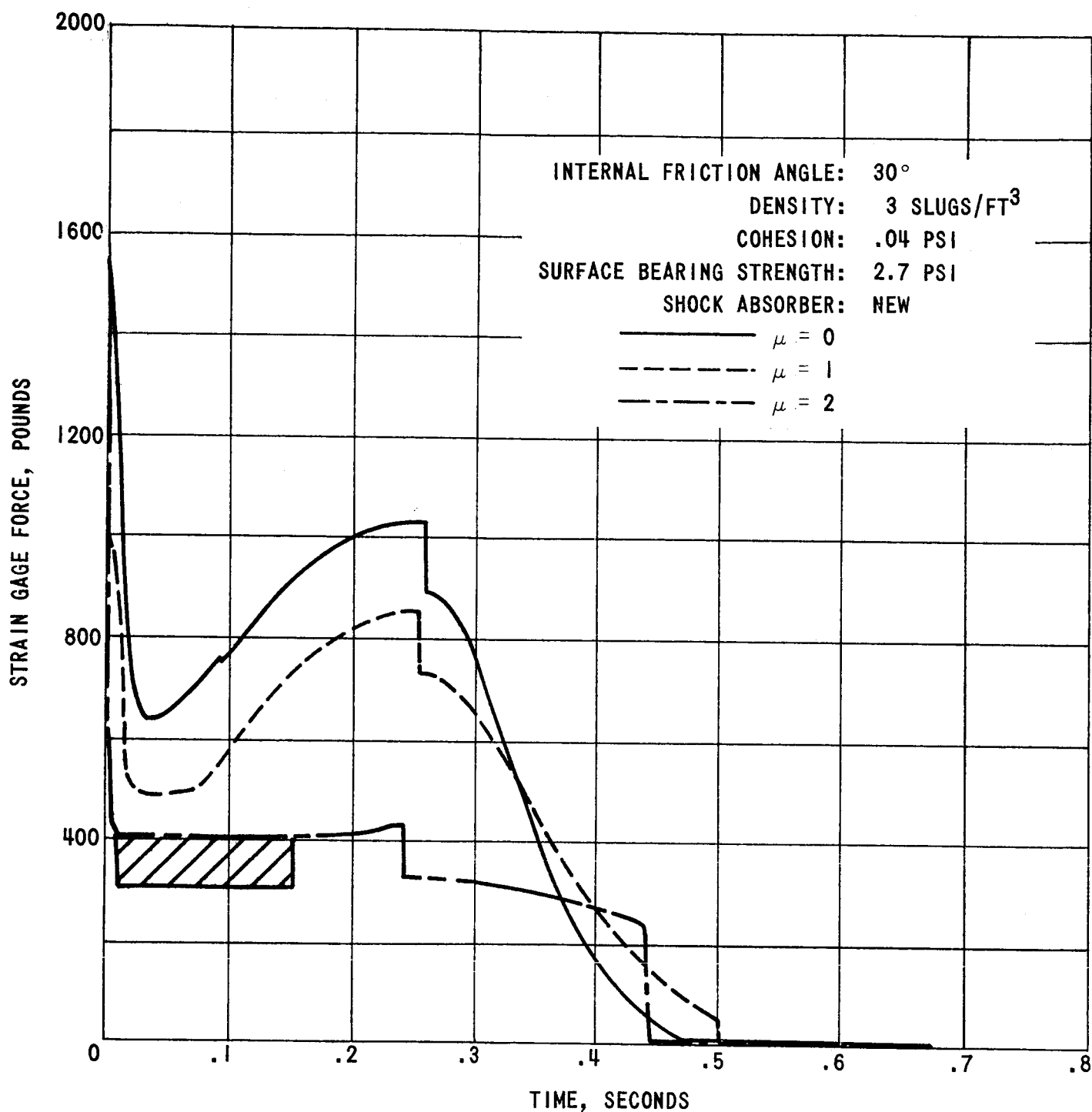


FIGURE 12 - VARIATION OF THE STRAIN GAGE TRACE DUE TO HORIZONTAL FORCES AT THE FOOTPAD. μ IS THE COEFFICIENT OF FRICTION. THE CROSS-HATCHING INDICATES A REGION OF OSCILLATION

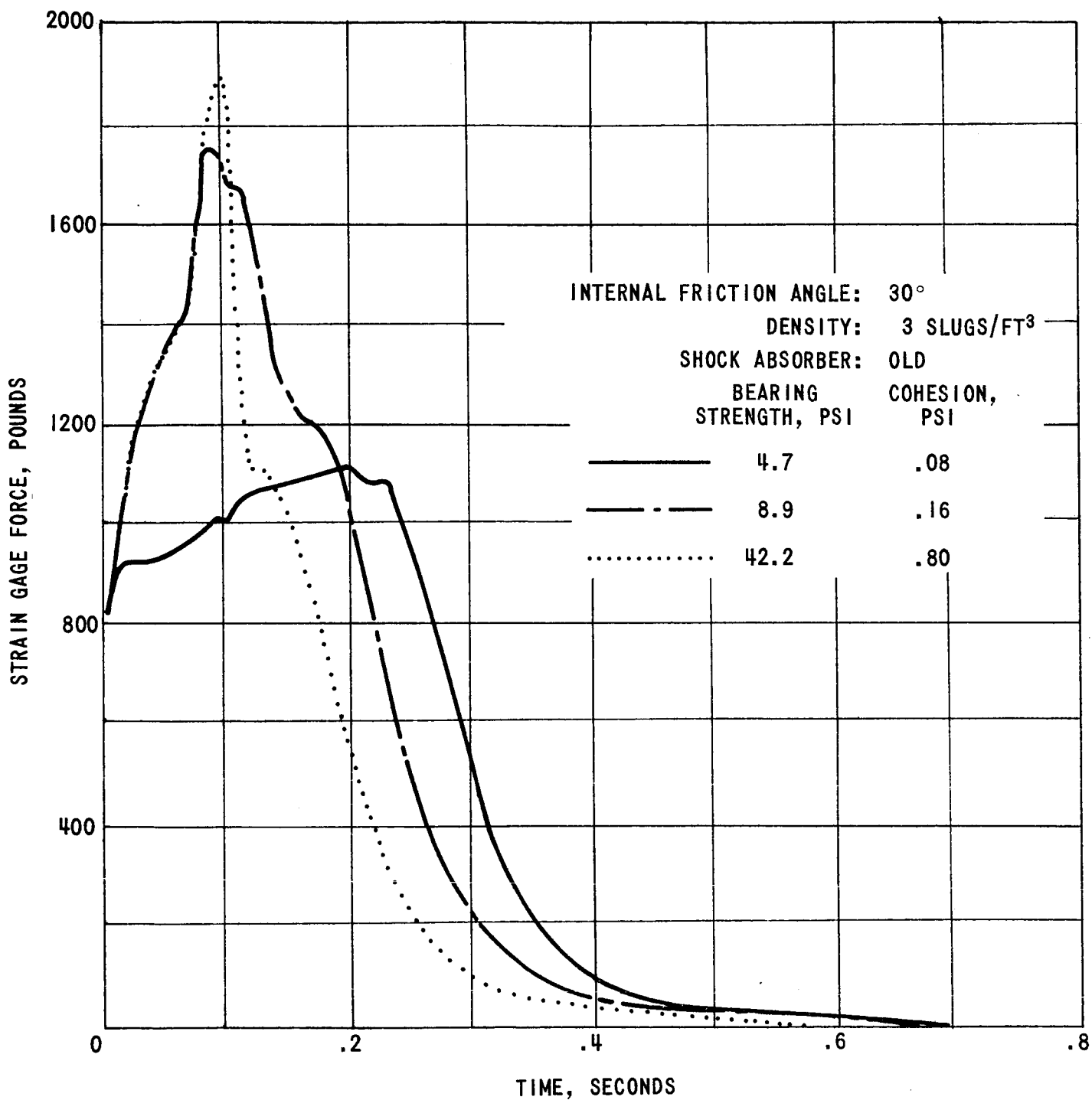


FIGURE 13 - COMPARISON OF STRAIN GAGE TRACES FOR THE OLD SHOCK ABSORBER ON SOILS OF DIFFERENT SURFACE STATIC BEARING CAPACITY

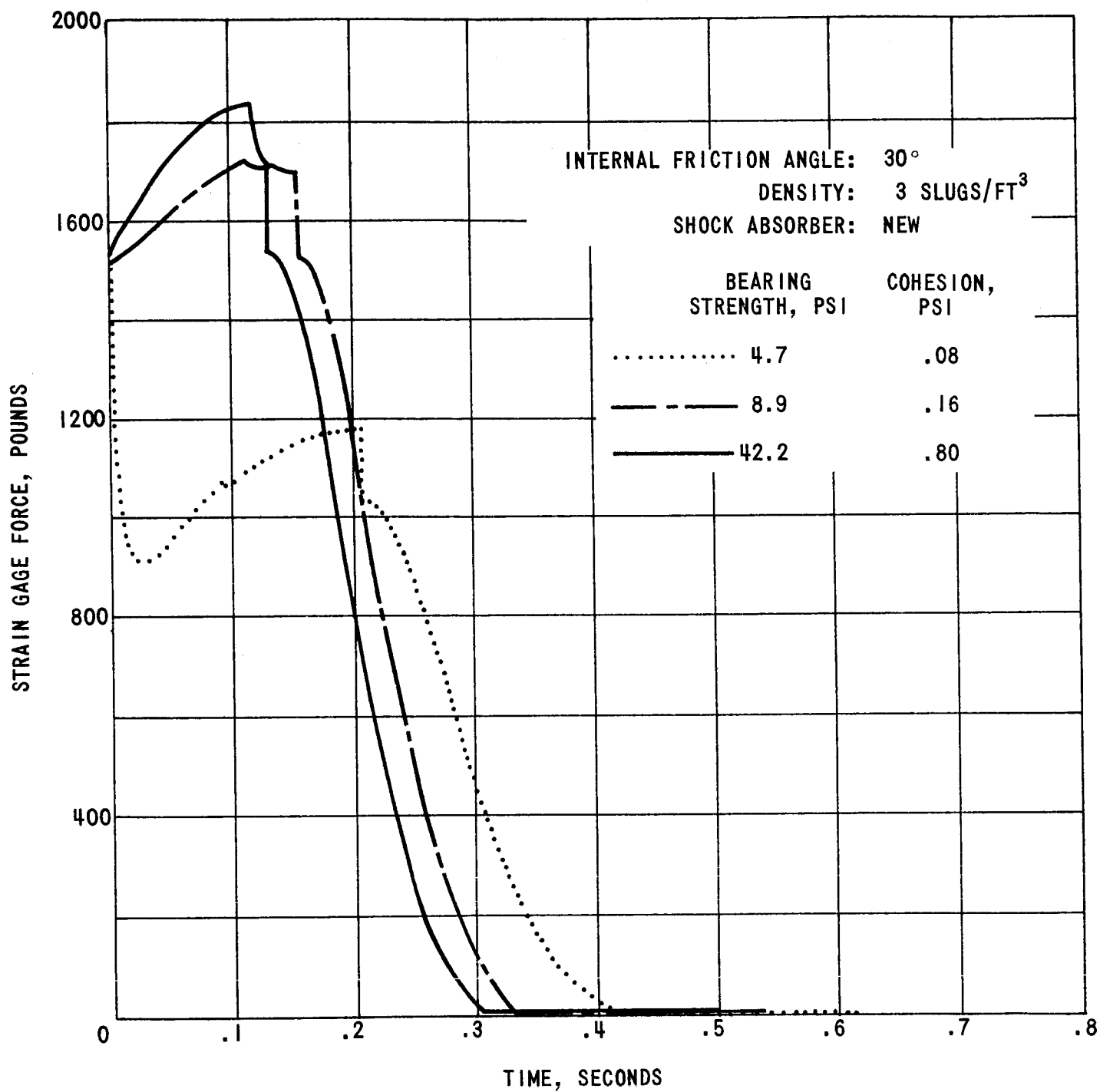


FIGURE 14 - COMPARISON OF STRAIN GAGE TRACES FOR THE NEW SHOCK ABSORBER ON SOILS OF DIFFERENT SURFACE STATIC BEARING CAPACITY

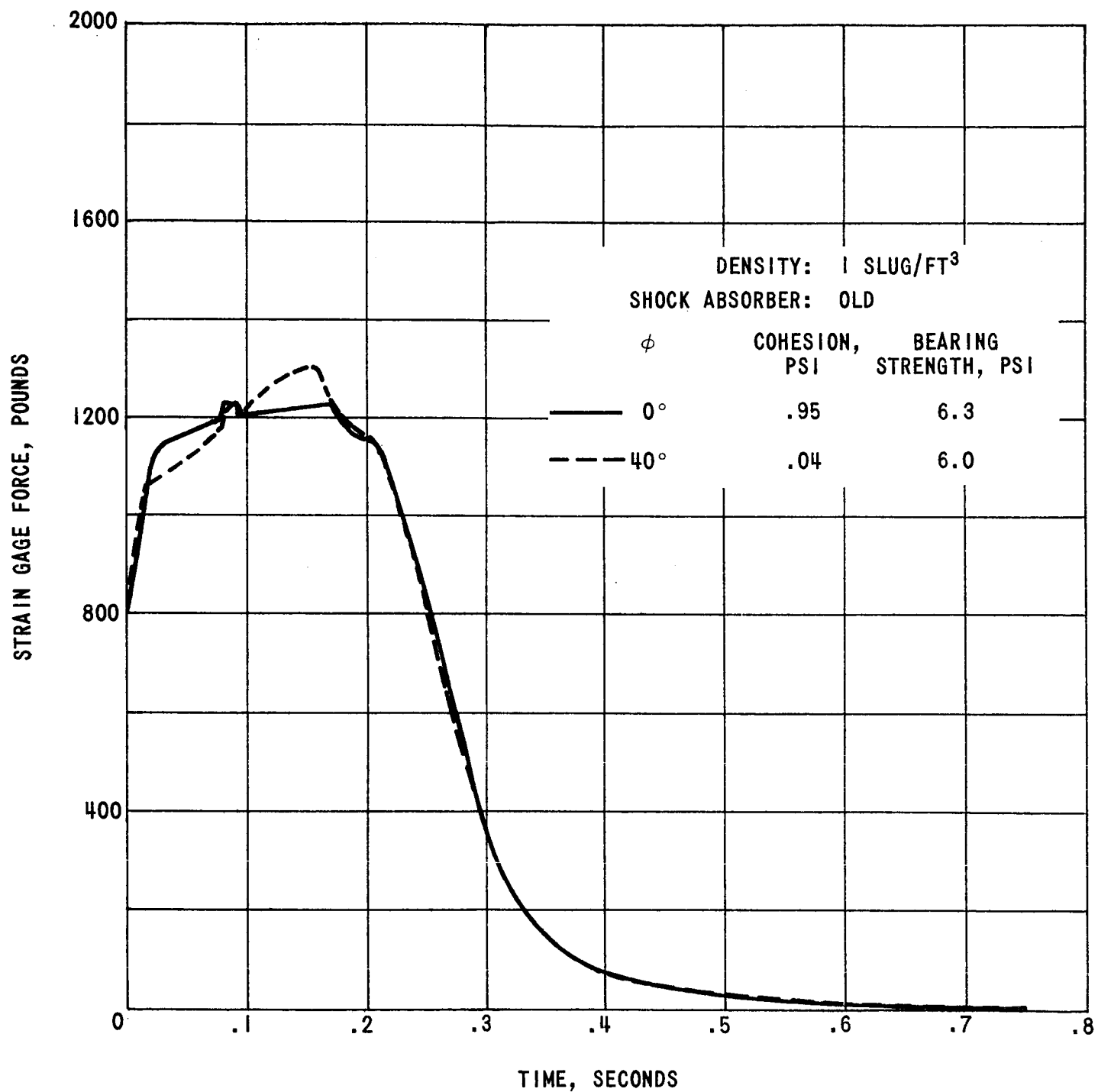


FIGURE 15 - VARIATION OF THE STRAIN GAGE TRACE FOR THE OLD SHOCK ABSORBER AS THE SOIL PARAMETERS ARE VARIED. ϕ IS THE INTERNAL FRICTION ANGLE. BOTH SETS OF SOIL PARAMETERS ARE CONSISTENT WITH SURVEYOR 1 FOOTPAD PENETRATION DATA (SEE TABLE II)

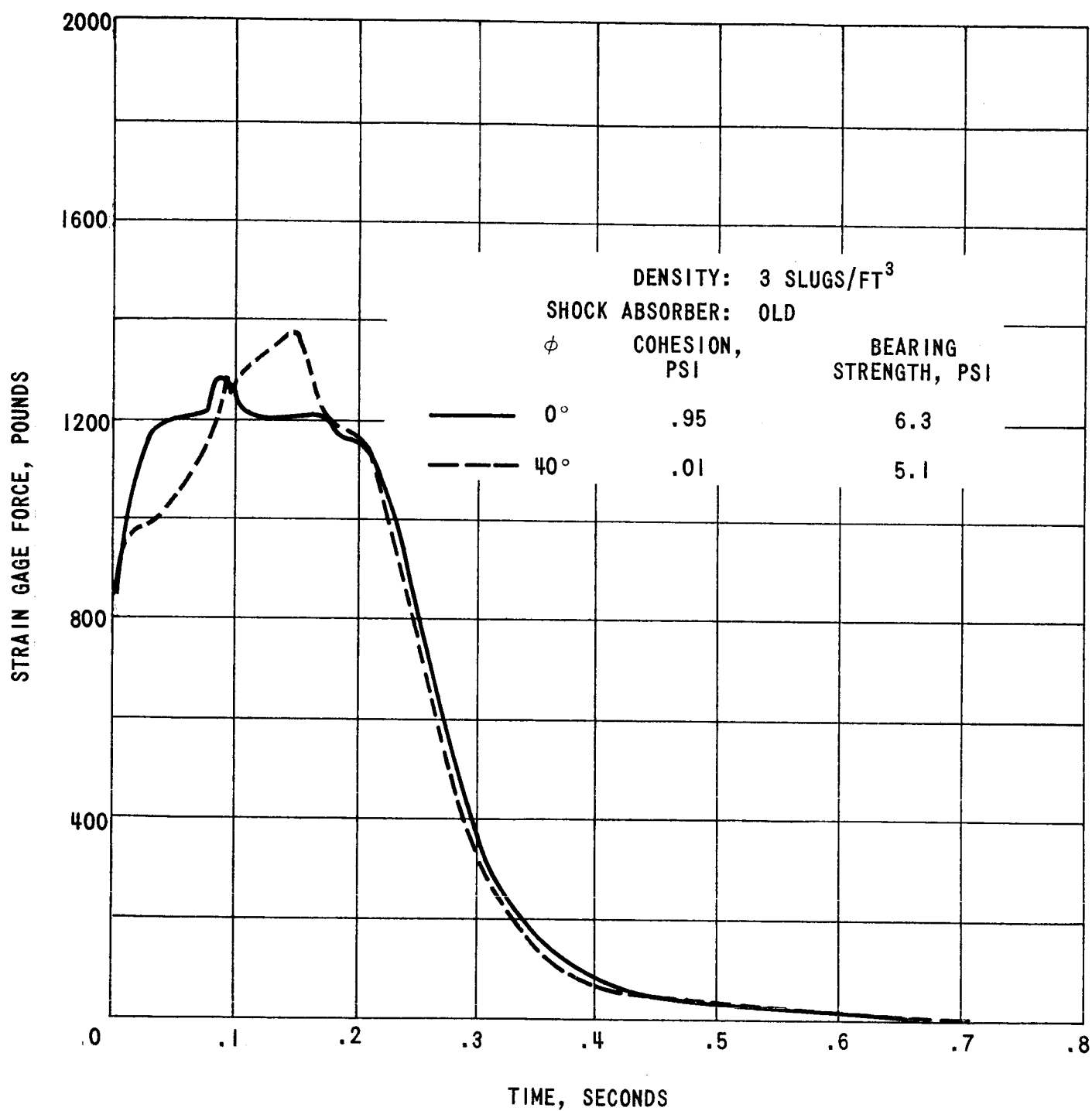


FIGURE 16 - VARIATION OF THE STRAIN GAGE TRACE FOR THE OLD SHOCK ABSORBER AS THE SOIL PARAMETERS ARE VARIED. ϕ IS THE INTERNAL FRICTION ANGLE. BOTH SETS OF SOIL PARAMETERS ARE CONSISTENT WITH SURVEYOR 1 PENETRATION DATA (SEE TABLE II)

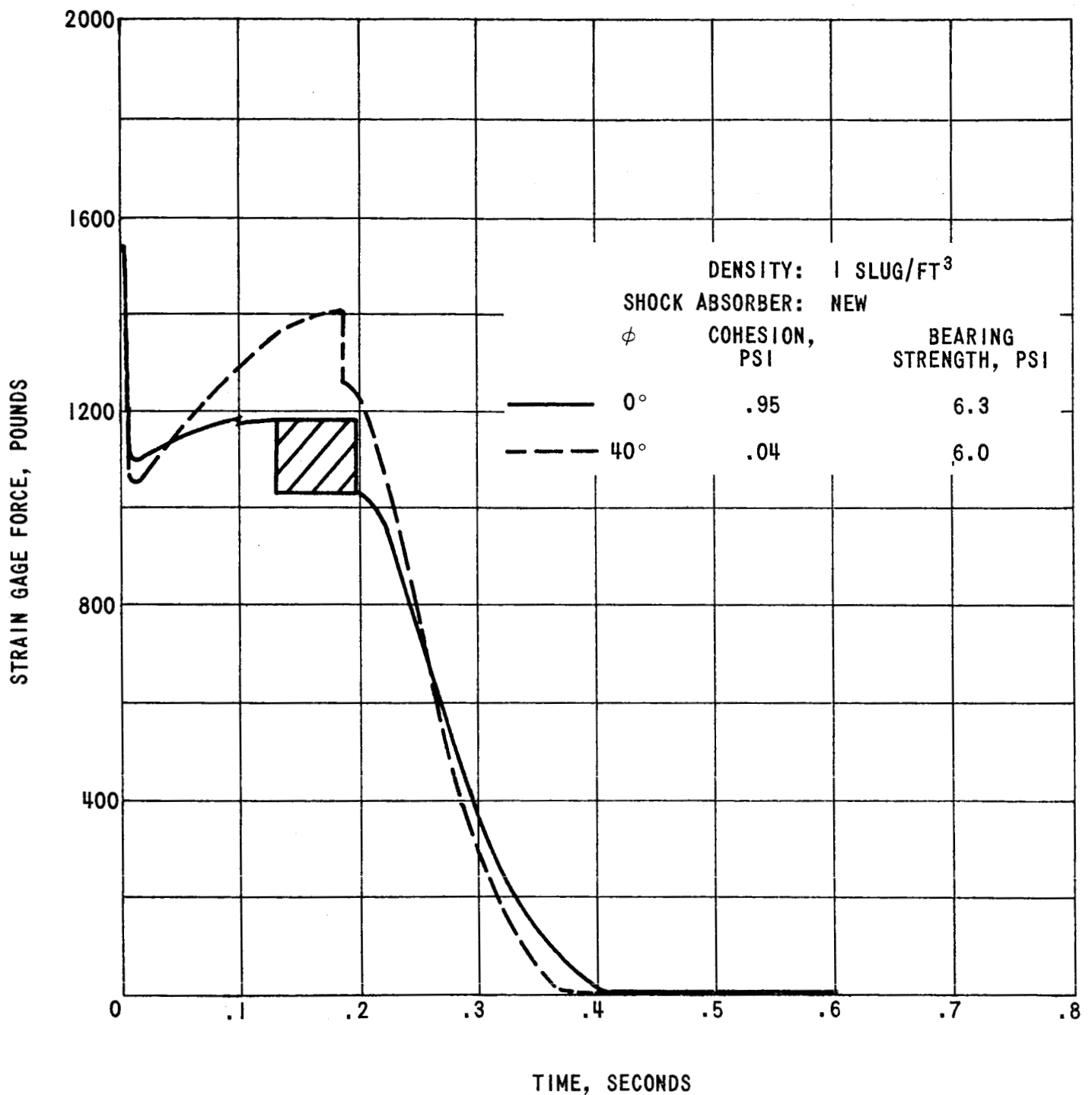


FIGURE 17 - VARIATION OF THE STRAIN GAGE TRACE FOR THE NEW SHOCK ABSORBER AS THE SOIL PARAMETERS ARE VARIED. ϕ IS THE INTERNAL FRICTION ANGLE. BOTH SETS OF SOIL PARAMETERS ARE CONSISTENT WITH SURVEYOR 1 FOOTPAD PENETRATION DATA (SEE TABLE II). THE CROSS HATCHING INDICATES A REGION OF OSCILLATION

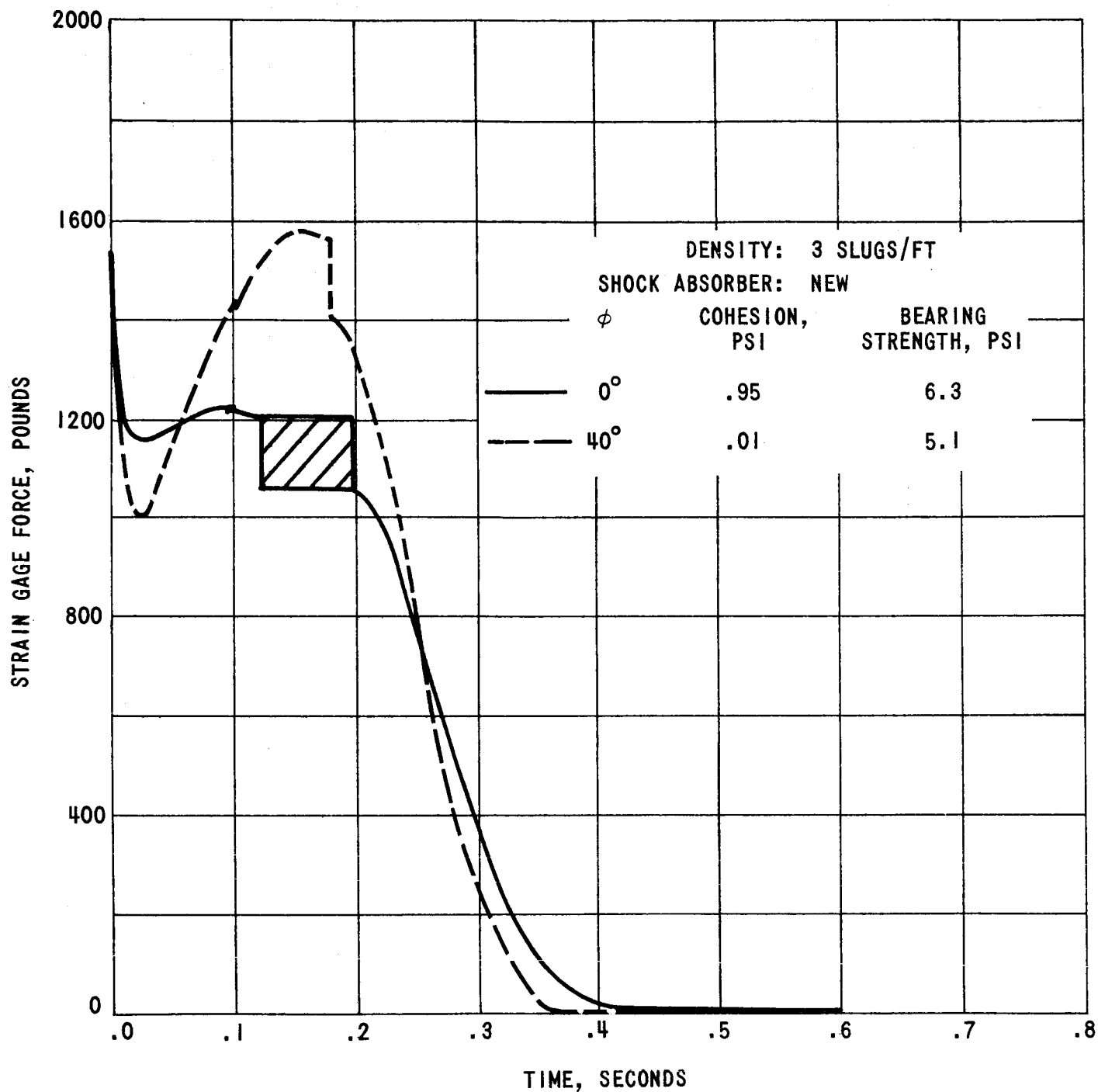


FIGURE 18 - VARIATION OF THE STRAIN GAGE TRACE FOR THE NEW SHOCK ABSORBER AS THE SOIL PARAMETERS ARE VARIED. ϕ IS THE INTERNAL FRICTION ANGLE. BOTH SETS OF SOIL PARAMETERS ARE CONSISTENT WITH SURVEYOR I FOOTPAD PENETRATION DATA (SEE TABLE II). THE CROSS HATCHING INDICATES A REGION OF OSCILLATION

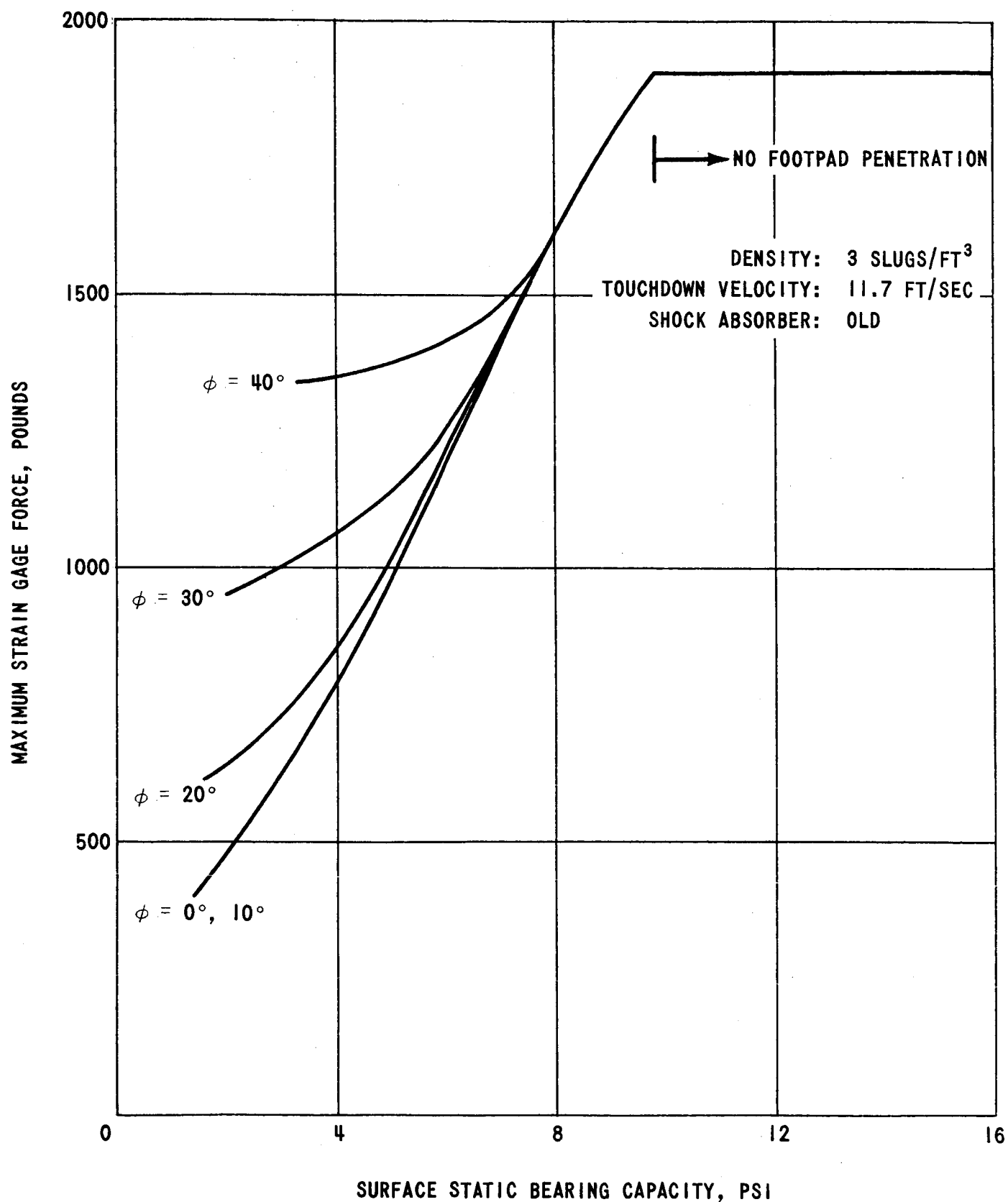


FIGURE 19 - THE PEAK STRAIN GAGE FORCE PLOTTED AS A FUNCTION OF THE SURFACE STATIC BEARING CAPACITY FOR VARIOUS VALUES OF THE INTERNAL FRICTION ANGLE ϕ . THESE CURVES ARE FOR THE OLD SHOCK ABSORBER. THE BEARING STRENGTH SCALE REFERS TO THE SURVEYOR FOOTPAD

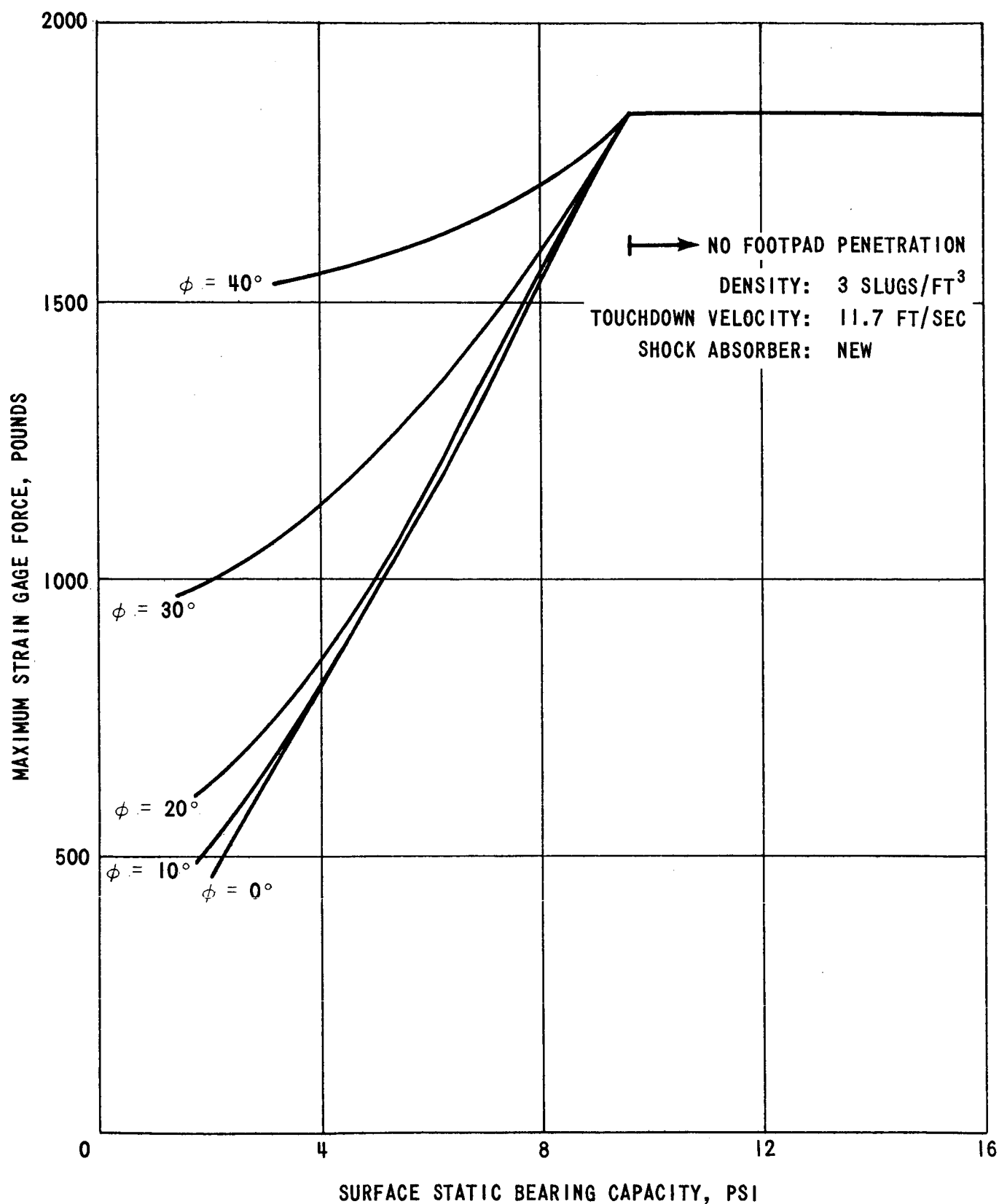


FIGURE 20 - THE PEAK STRAIN GAGE FORCE PLOTTED AS A FUNCTION OF THE SURFACE STATIC BEARING CAPACITY FOR VARIOUS VALUES OF THE INTERNAL FRICTION ANGLE ϕ . THESE CURVES ARE FOR THE NEW SHOCK ABSORBER. THE BEARING CAPACITY SCALE REFERS TO THE SURVEYOR FOOTPAD

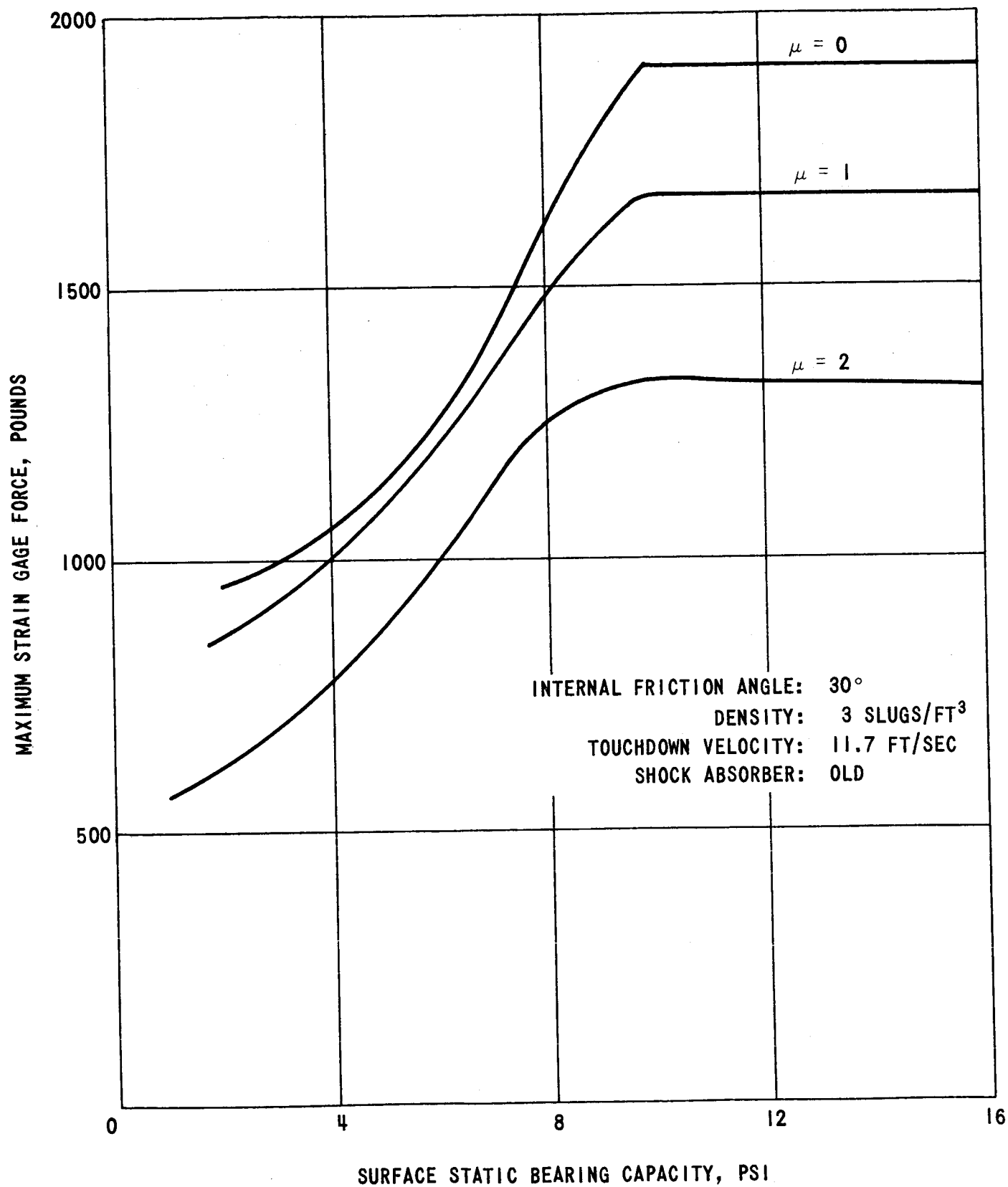


FIGURE 21 - EFFECT OF HORIZONTAL FORCES AT THE FOOTPAD ON THE MAXIMUM STRAIN GAGE FORCE. μ IS THE COEFFICIENT OF FRICTION BETWEEN THE FOOTPAD AND THE SURFACE. THE BEARING CAPACITY SCALE REFERS TO THE SURVEYOR FOOTPAD

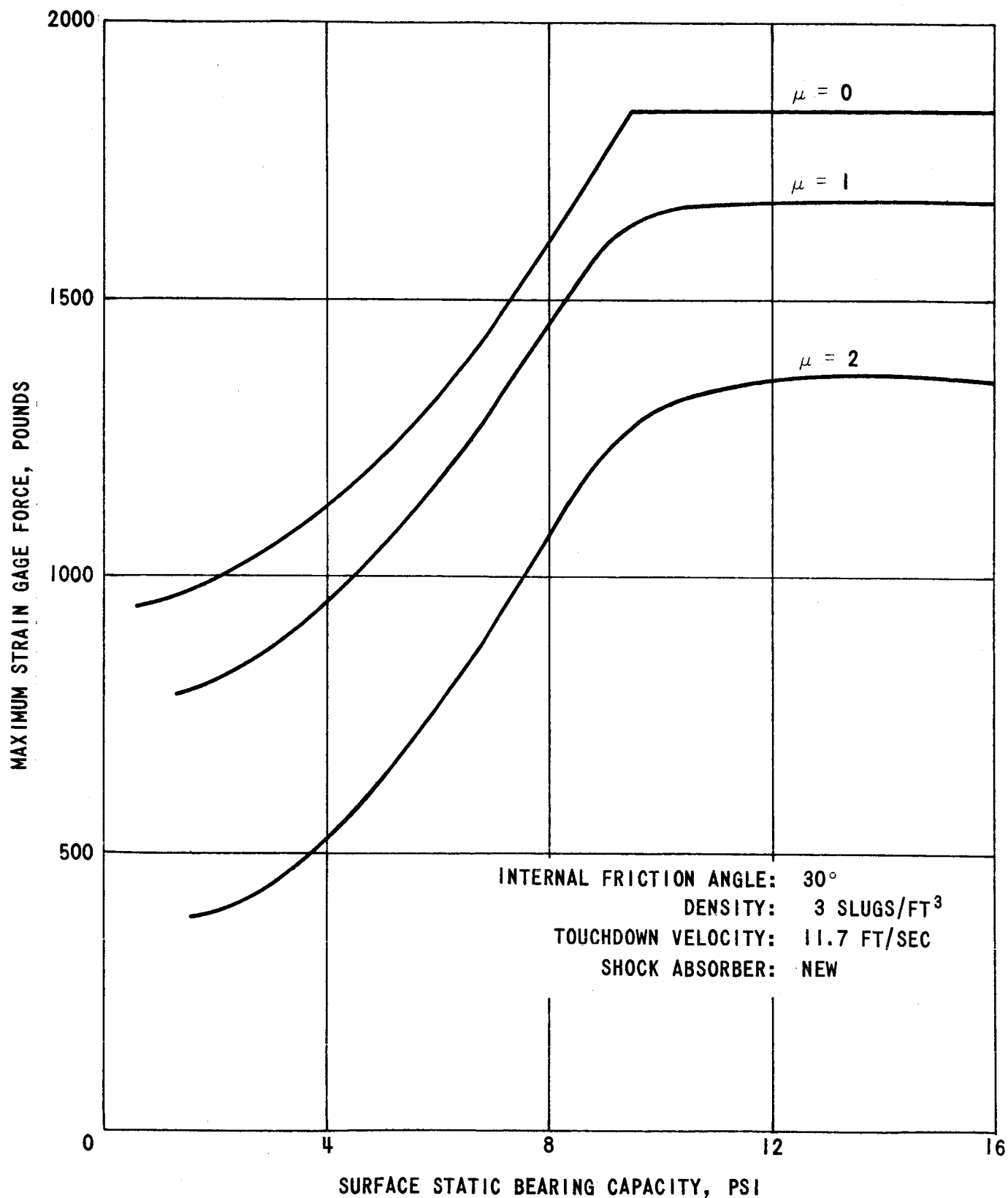


FIGURE 22 - EFFECT OF HORIZONTAL FORCES AT THE FOOTPAD ON THE MAXIMUM STRAIN GAGE FORCE. μ IS THE COEFFICIENT OF FRICTION BETWEEN THE FOOTPAD AND THE SURFACE. THE BEARING CAPACITY SCALE REFERS TO THE SURVEYOR FOOTPAD

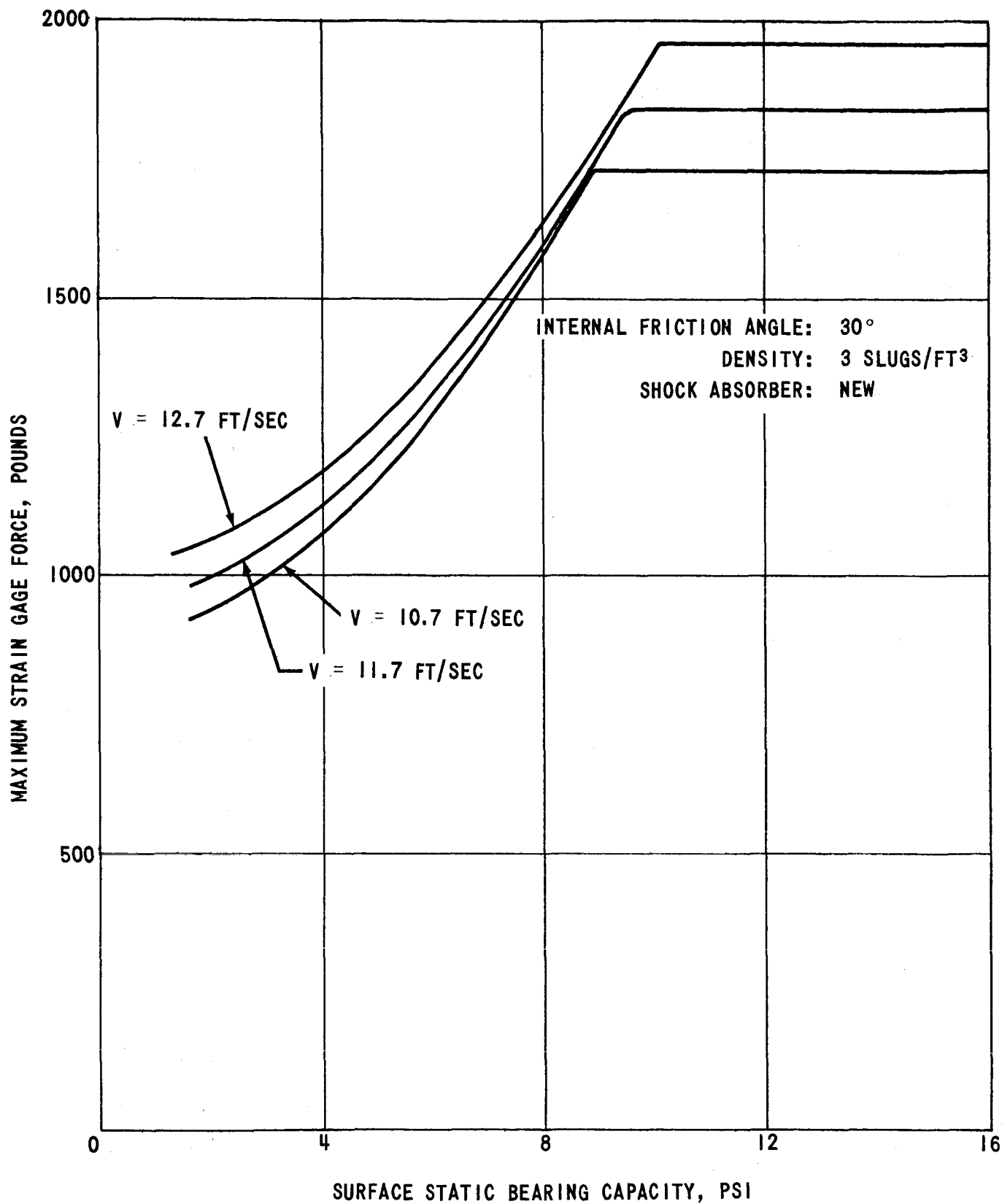


FIGURE 23 - THE EFFECT OF THE TOUCHDOWN VELOCITY, V , ON THE MAXIMUM STRAIN GAGE FORCE FOR THE NEW SHOCK ABSORBER. THE BEARING STRENGTH SCALE REFERS TO THE SURVEYOR FOOTPAD.

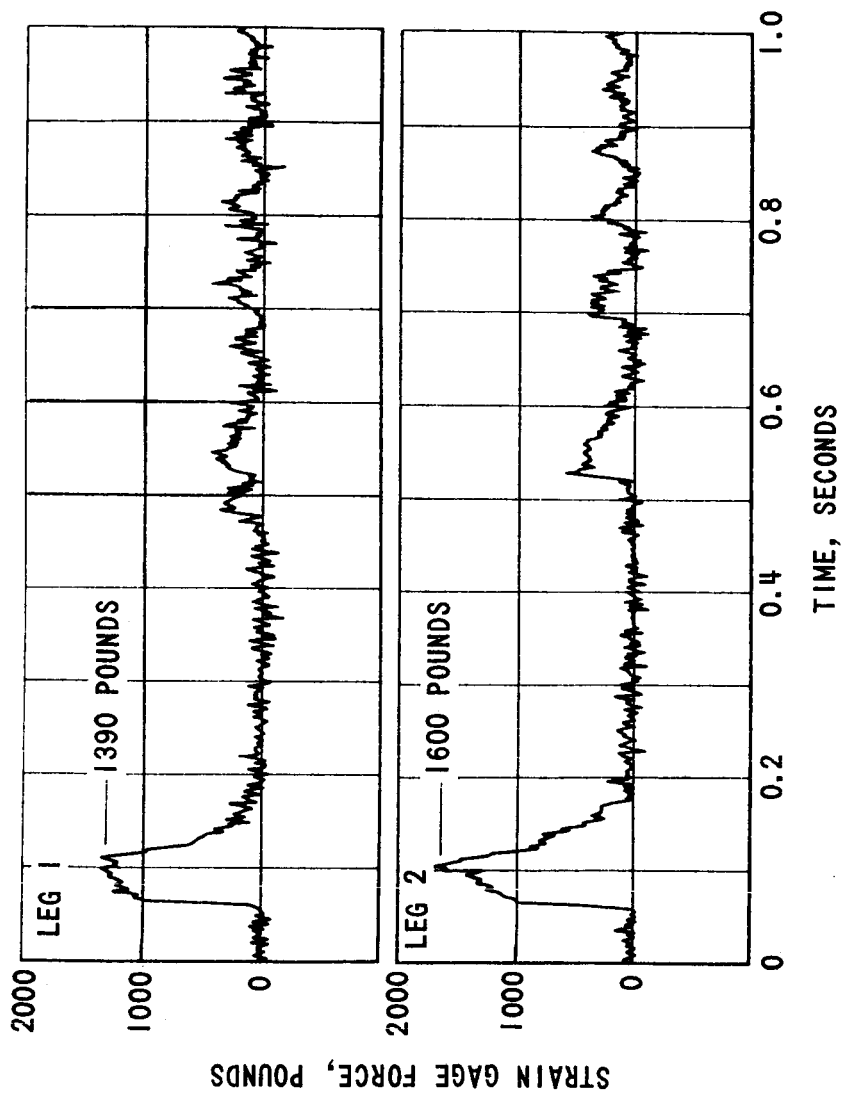


FIGURE 24 - ORIGINAL SURVEYOR 1 STRAIN GAGE TRACES.
THE CURVE FOR LEG 3 IS NOT INCLUDED
BECAUSE OF CALIBRATION UNCERTAINTIES
(SEE REFERENCE 3)

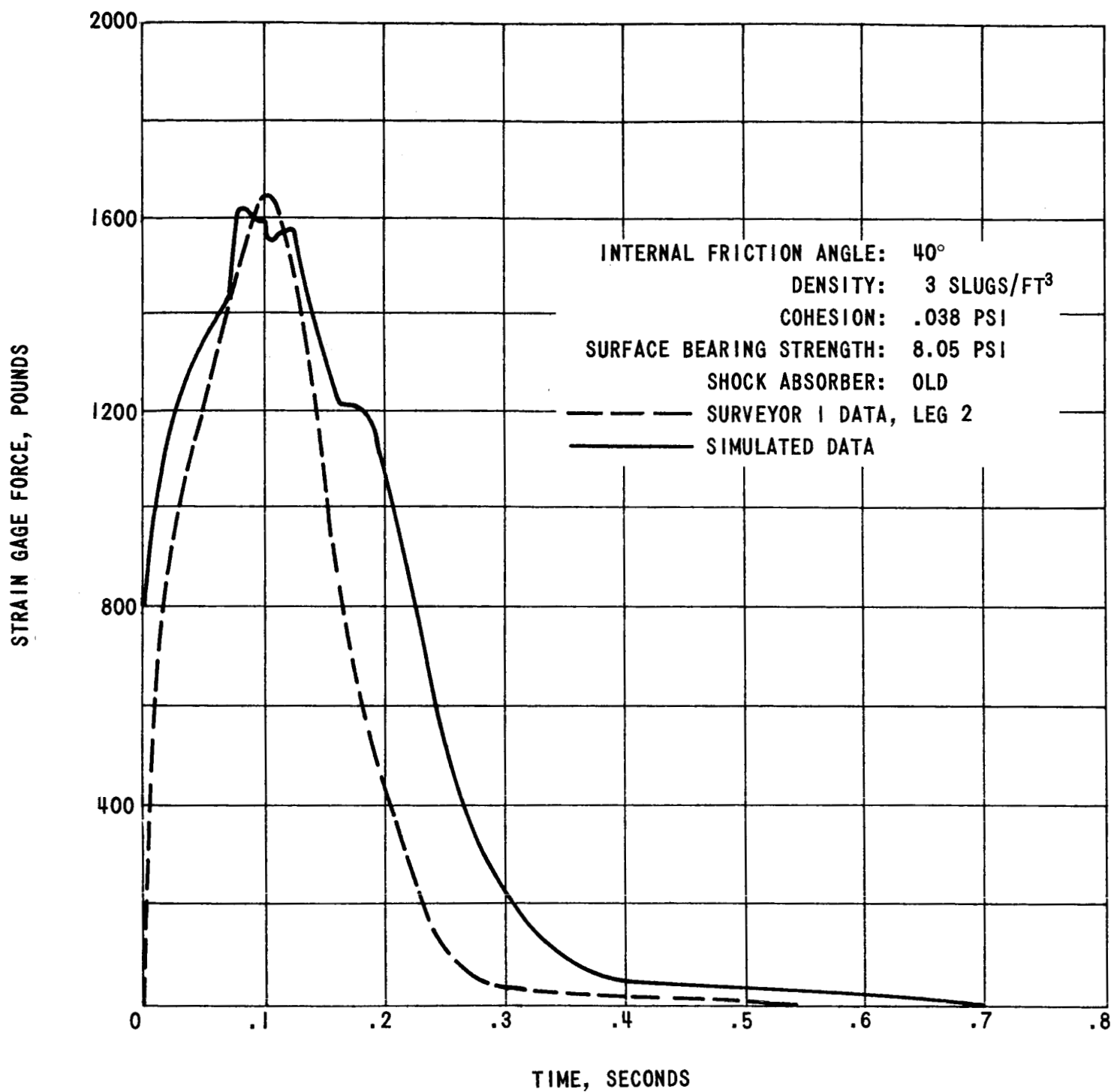


FIGURE 25 - COMPARISON OF SURVEYOR 1 DATA WITH SIMULATED STRAIN GAGE DATA

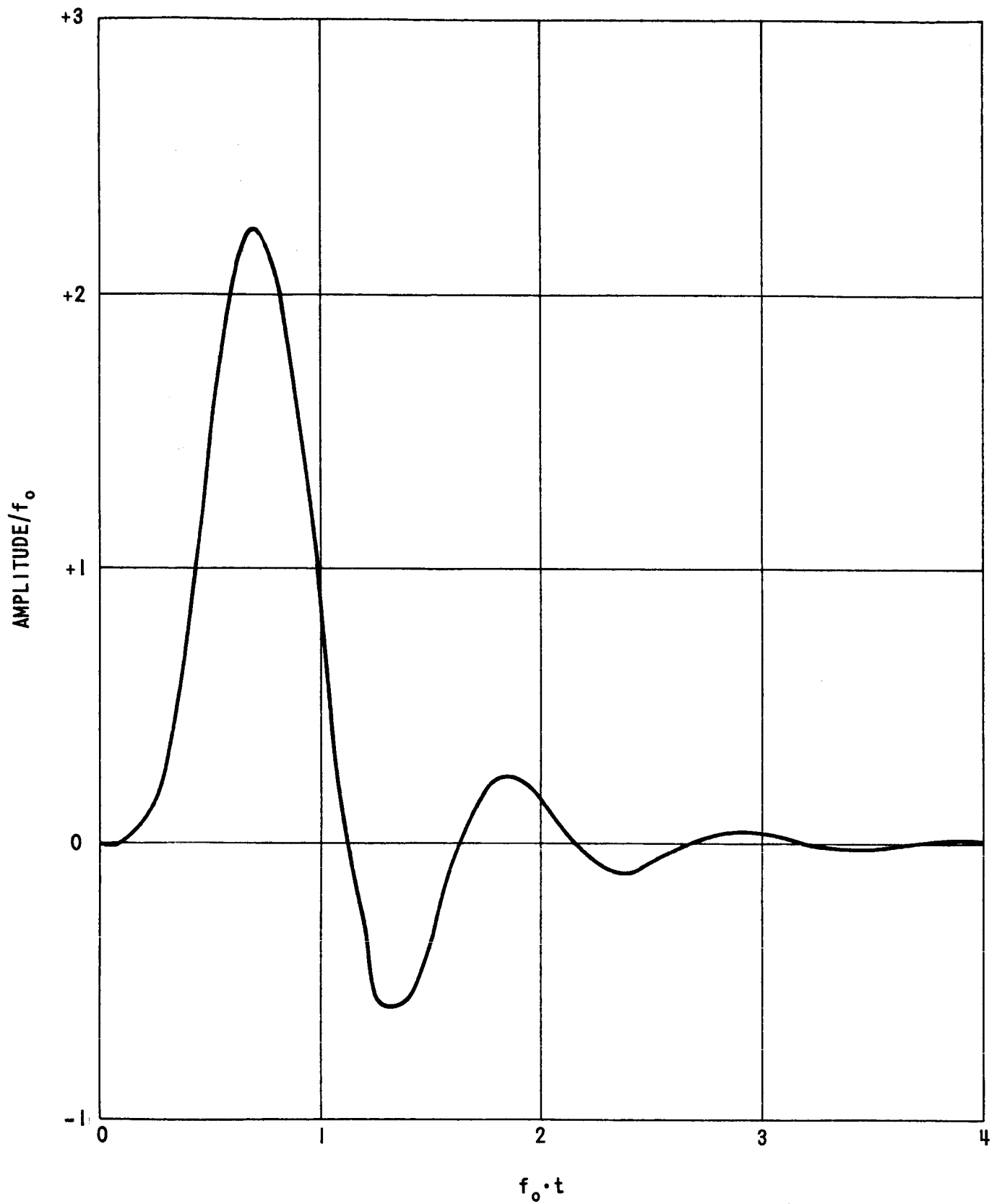


FIGURE 26 - IMPULSE RESPONSE FUNCTION OF A 6th ORDER BUTTERWORTH FILTER. NOTICE THAT BOTH THE AMPLITUDE AND THE TIME BASE DEPEND ON THE CUTOFF FREQUENCY f_0 . t IS THE TIME IN SECONDS, AND f_0 IS IN Hz

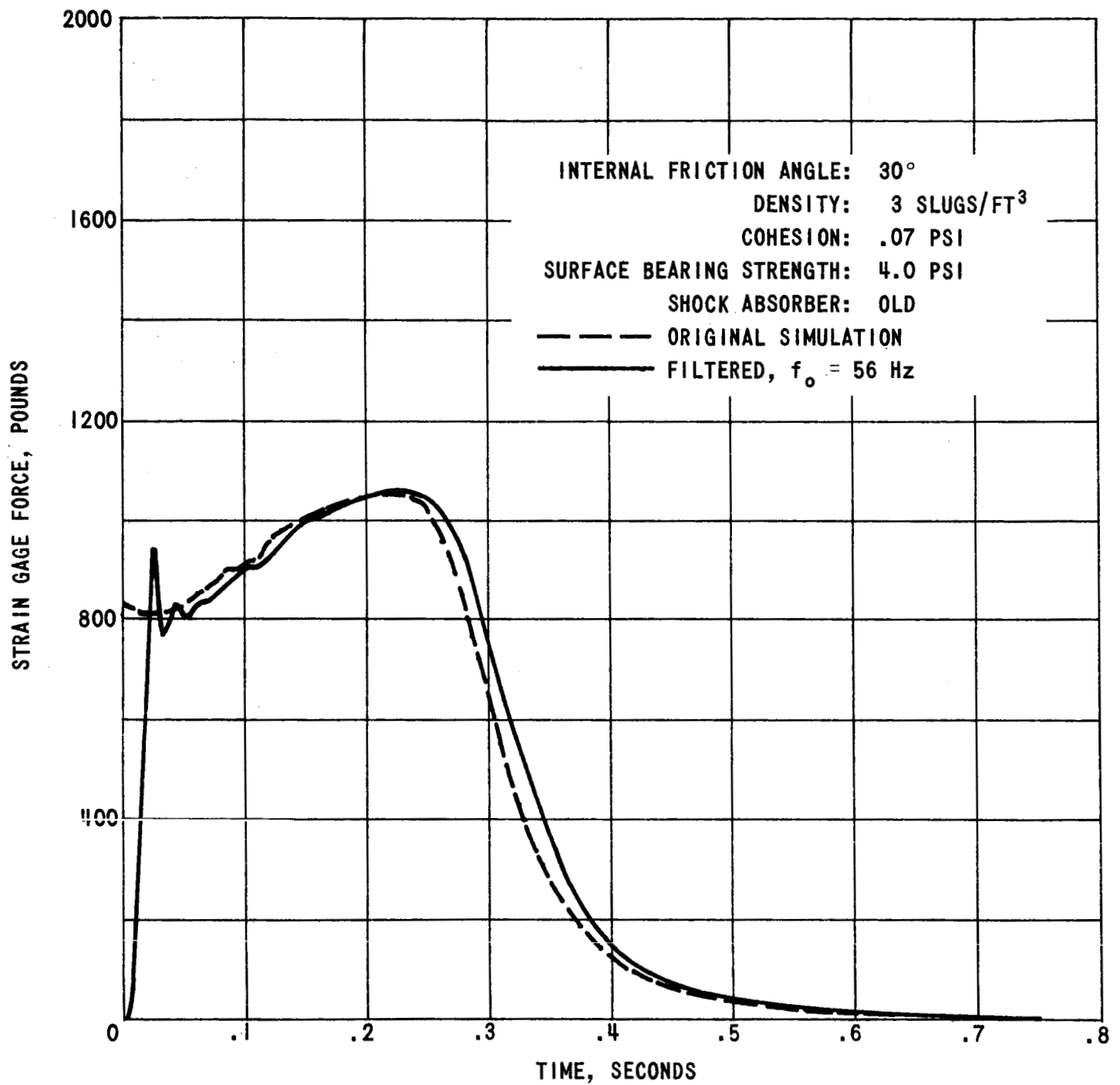


FIGURE 27 - EFFECT OF THE FILTER ON THE STRAIN GAGE TRACE FOR THE OLD SHOCK ABSORBER. THE CUTOFF FREQUENCY f_o IS 56 Hz

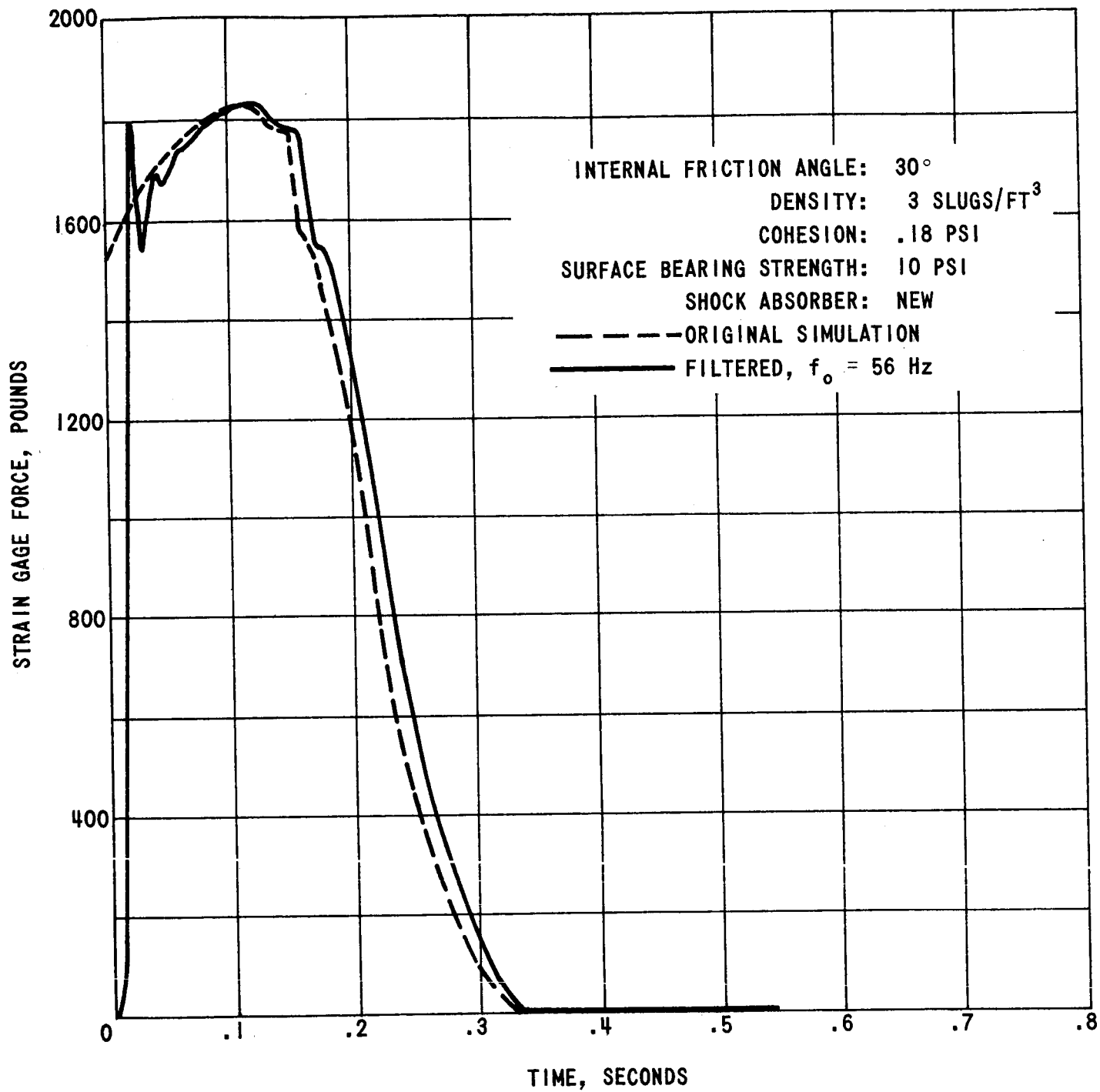


FIGURE 28 - EFFECT OF THE FILTER ON THE STRAIN GAGE TRACE FOR THE NEW SHOCK ABSORBER. THE CUTOFF FREQUENCY f_o IS 56 Hz

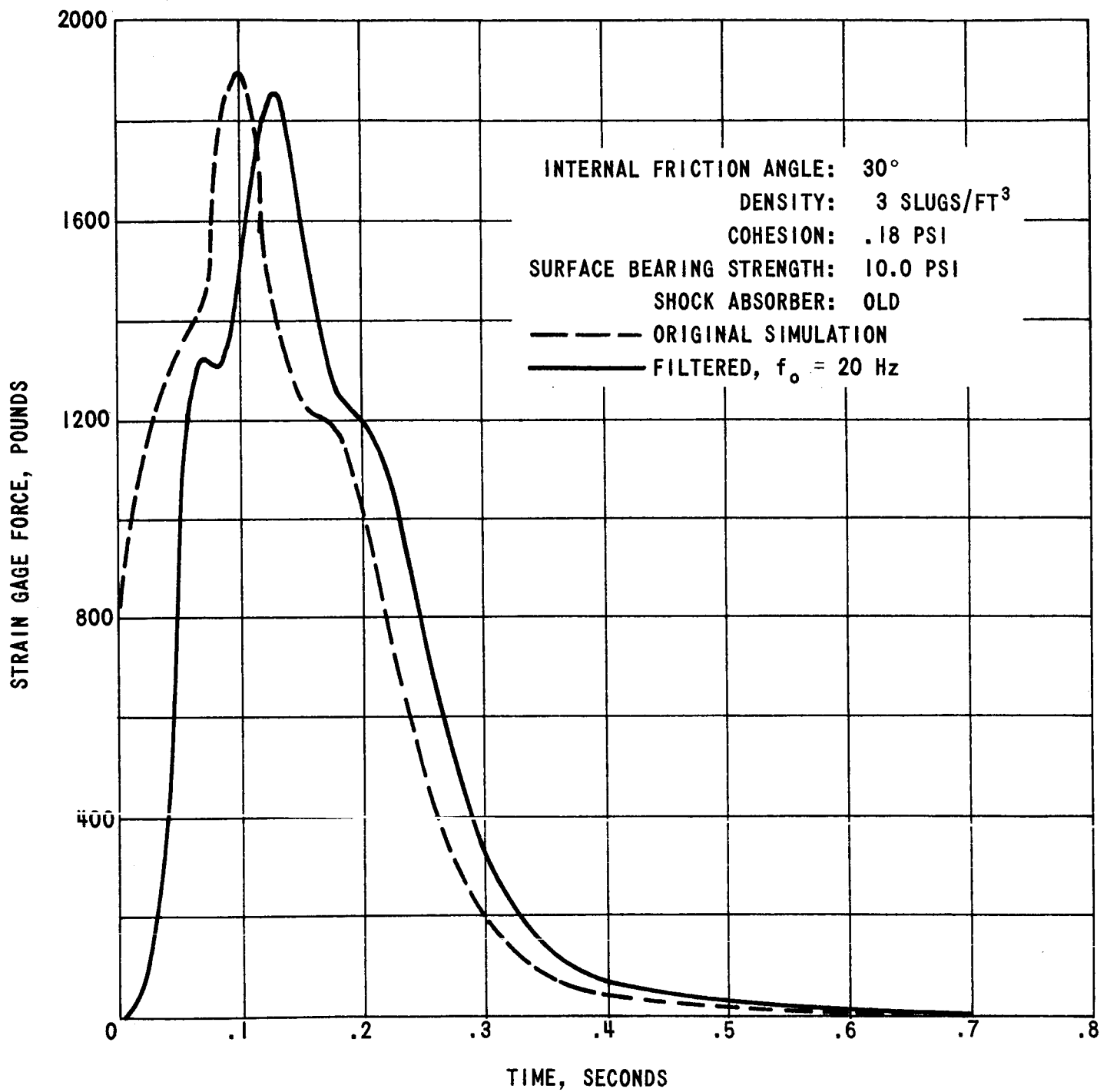


FIGURE 29 - EFFECT OF THE FILTER ON THE STRAIN GAGE TRACE FOR THE OLD SHOCK ABSORBER. THE CUTOFF FREQUENCY f_o IS 20 Hz

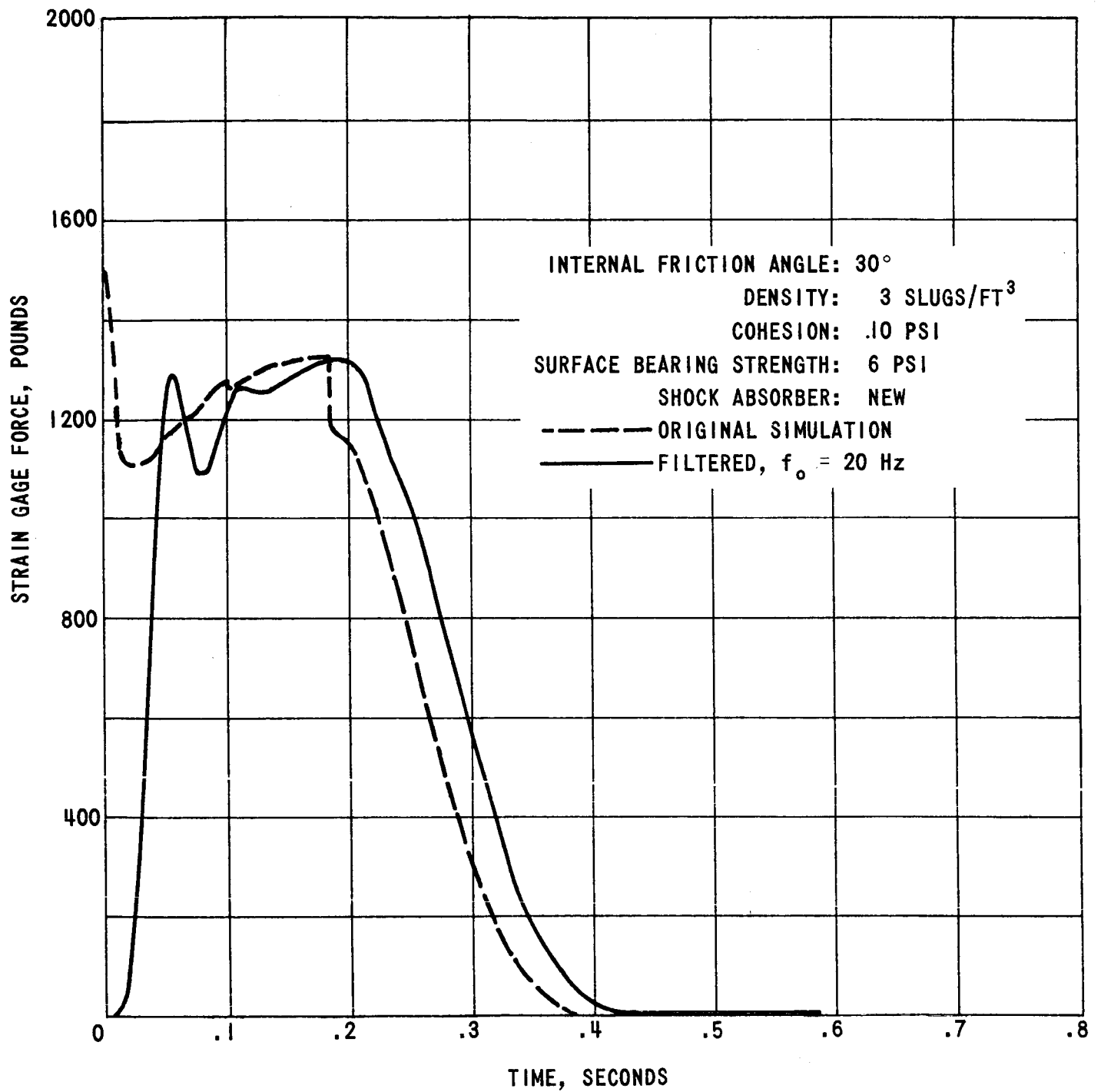


FIGURE 30 - EFFECT OF THE FILTER ON THE STRAIN GAGE TRACE FOR THE NEW SHOCK ABSORBER. THE CUTOFF FREQUENCY f_0 IS 20 Hz

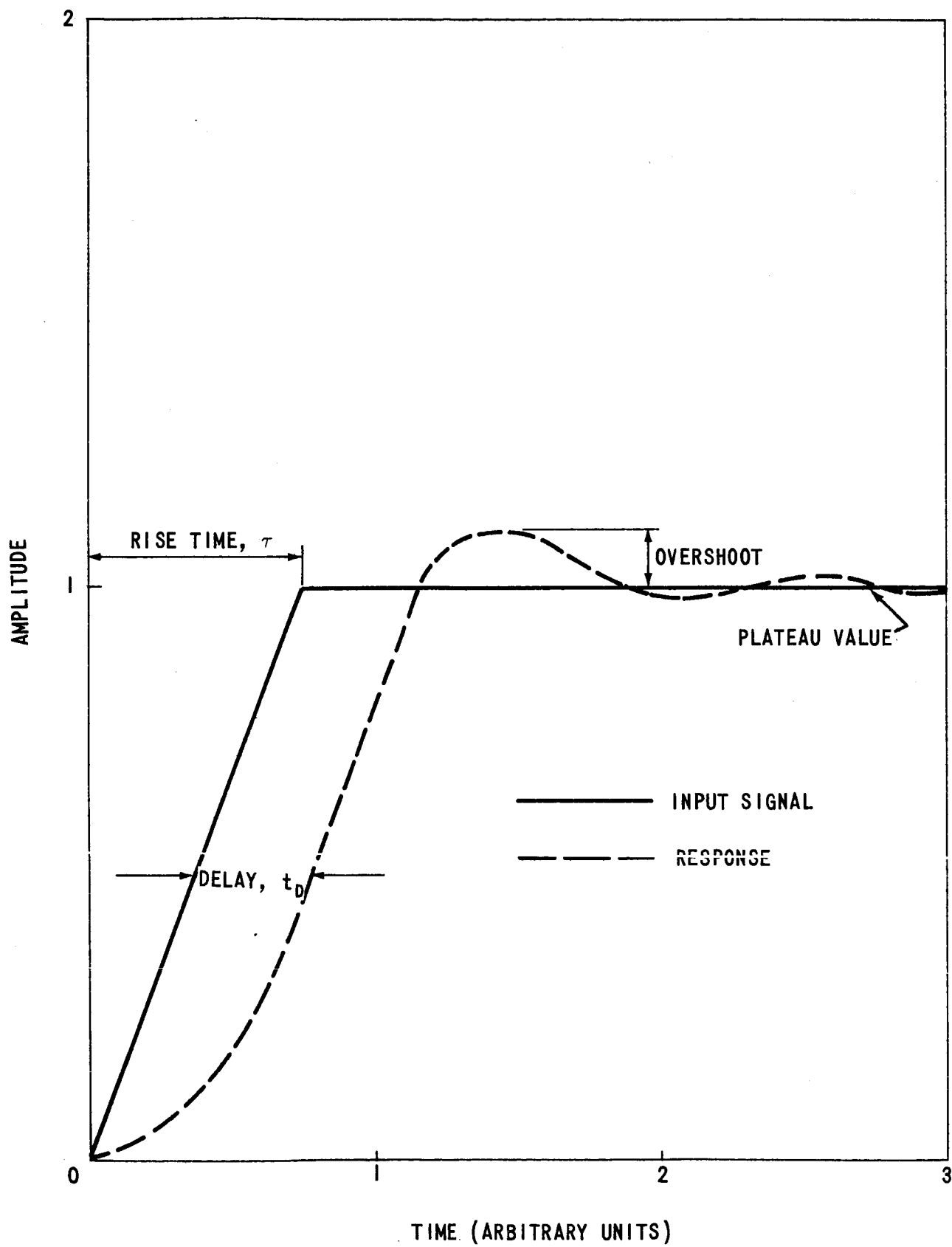


FIGURE 31 - STANDARD FUNCTION USED IN THE OVERSHOOT STUDY

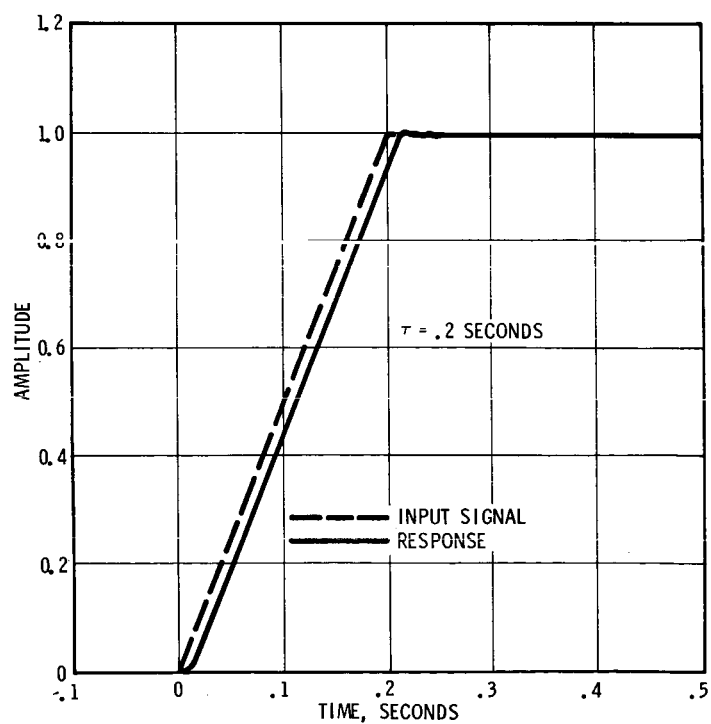
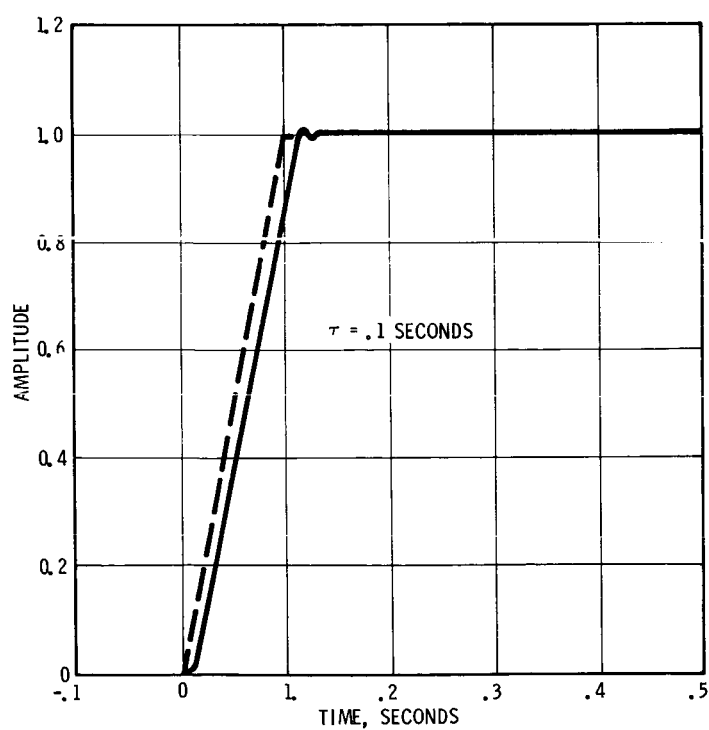
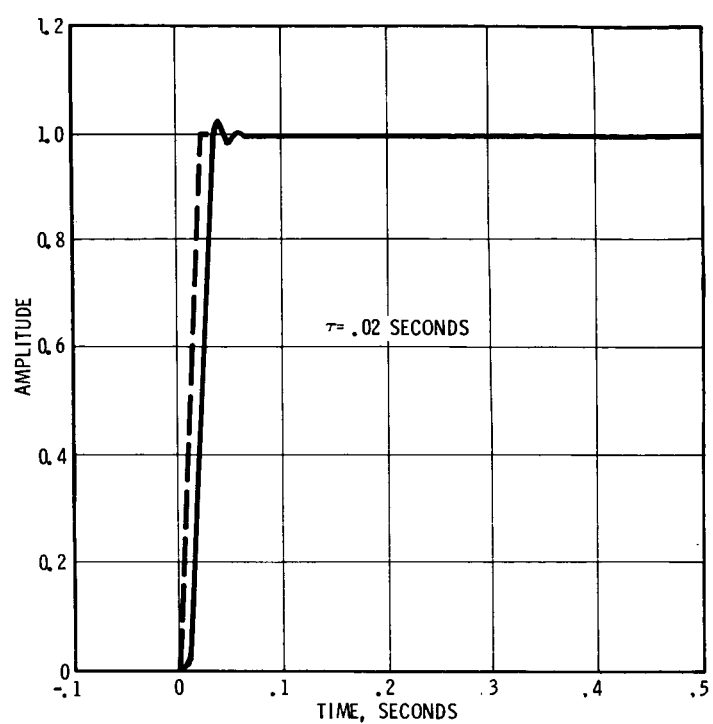
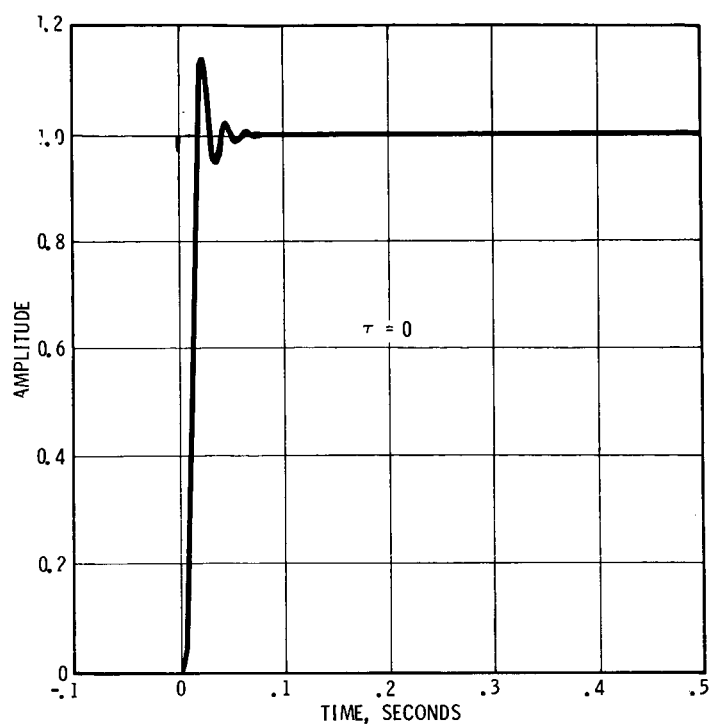


FIGURE 32 - FILTERED OUTPUT FOR STANDARD INPUT (RAMP) SIGNAL. SEE FIGURE 31 FOR TERMINOLOGY. THE CUTOFF FREQUENCY OF THE FILTER WAS 50 Hz

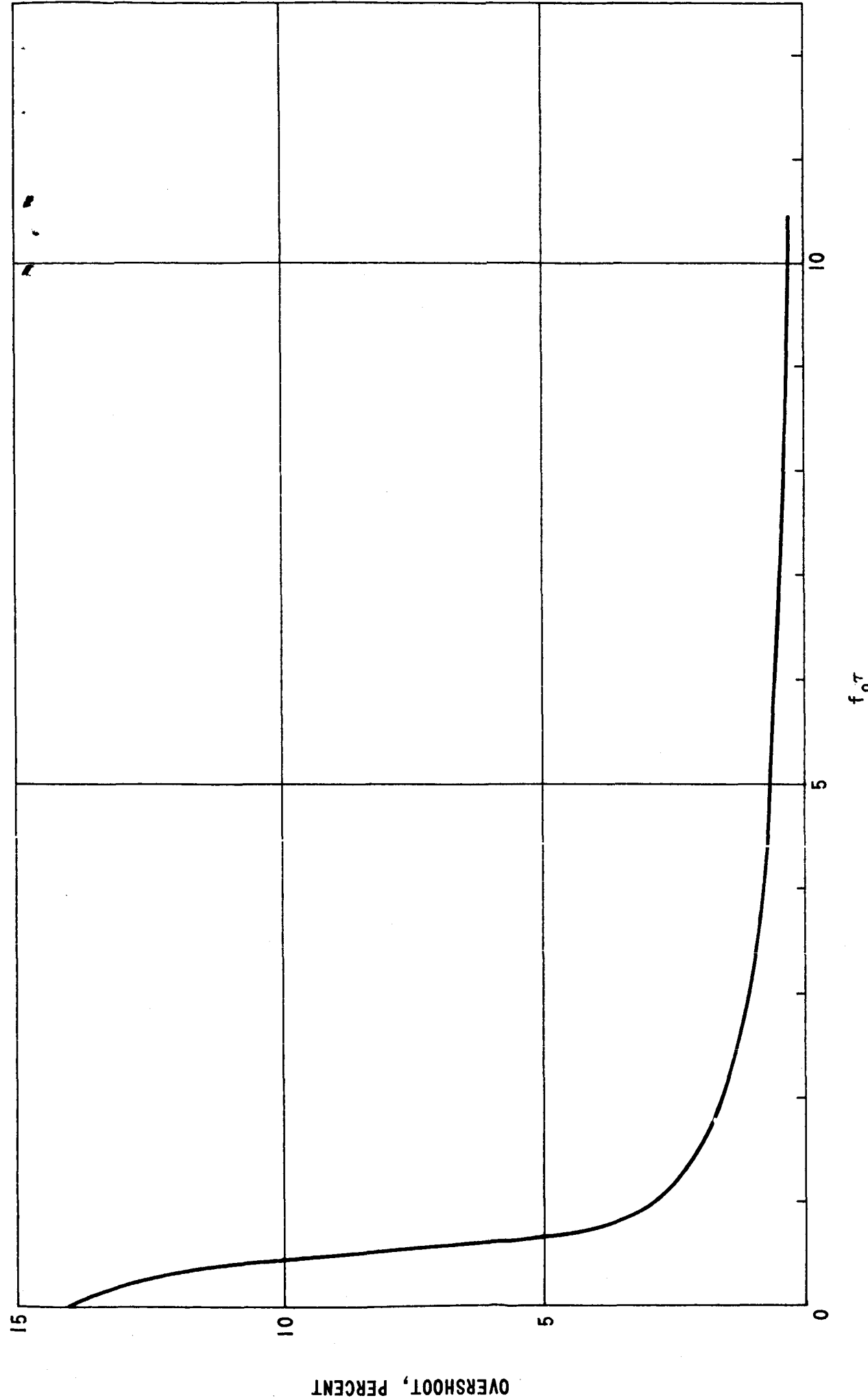


FIGURE 33 - OVERSHOOT VERSUS $f_o \tau$. f_o IS THE FILTER CUTOFF FREQUENCY (IN Hz.) AND τ IS THE RISE TIME OF THE RAMP FUNCTION (IN SECONDS). OVERSHOOT IS EXPRESSED AS A PERCENT OF THE PLATEAU VALUE OF THE INPUT SIGNAL. SEE FIGURE 31 FOR AN ILLUSTRATION OF THE INPUT AND RESPONSE SIGNAL